Kusebauch, C., John, T., Whitehouse, M. J., Engvik, A. (2015): Apatite as probe for the halogen composition of metamorphic fluids (Bamble Sector, SE Norway). - *Contributions to Mineralogy and Petrology*, *170*.

DOI: http://doi.org/10.1007/s00410-015-1188-6

# Apatite as probe for the halogen composition of metamorphic fluids (Bamble Sector SE Norway)

Christof Kusebauch[1,5+], Timm John[2], Martin J. Whitehouse[3], Ane K. Engvik[4]

[1]Institut für Mineralogie, Westfälische Wilhelms-Universität Münster, Corrensstr. 24, D-48149 Münster, Germany

[2]Institut für geologische Wissenschaften, Freie Universität Berlin, Malteser Str. 74-100, 12249 Berlin, Germany

[3]Swedish Museum of Natural History, P. O. Box 50007, SE-104 05 Stockholm, Sweden

[4]Geological Survey of Norway, P.O.Box 6315 Sluppen, N-7491 Trondheim, Norway

[5]Deutsches GeoForschungsZentrum Potsdam, Telegrafenberg, D-14473 Potsdam, Germany

[+]corresponding author: Christof Kusebauch, c.kusebauch@uni-muenster.de,

fax +49 251 83 38397

phone +49 251 83 33506

## Abstract

Halogen composition of replaced apatite formed during a regional metasomatic event (Bamble Sector SE Norway) reveals information about the composition and evolution of the hydrothermal fluid. Infiltration and pervasive fluid flow of highly saline fluids into gabbroic bodies lead to scapolitization and amphibolitization, where magmatic Cl-rich apatite reacts with the hydrothermal fluid to form OH- and/or F-rich apatite. Apatite from highly altered samples adjacent to the shear zone has highest F (up to 15000 µg/g) and lowest Br (4-25 µg/g) concentrations, whereas apatite from least altered samples has very low F (30-200 µg/g) and high Br (30-85 µg/g). In addition, individual replaced apatite grains show a zonation in F with high concentrations along rims and cracks and low F in core regions. Iodine concentrations remain rather constant as low values of 0.18-0.70 µg/g. We interpret all observed compositional features of replaced apatite to be the result of a continuous evolution of the fluid during fluid-rock interaction. Due to its high compatibility, F from the infiltrating fluid is incorporated early into recrystallized apatite (close to shear zone and rims of individual apatite grains). In contrast, Br as an incompatible halogen becomes enriched in the fluid and is highest in the most evolved fluid. Using experimental partition data between replaced apatite and fluid, we calculated F concentrations of the evolving fluid to decrease from 60 to <1 µg/g and Br to increase from ~1500 to ~ 6500 µg/g; I concentrations of the fluid are constant in the order of 300µg/g. Although, Cl is expected to show a similar behavior as Br, replaced apatite has constant Cl concentrations throughout the alteration sequence (~1 wt.%), which is likely the result of a rather constant Cl activity in the fluid. Chlorine stable isotope values of individual apatite grains are heterogeneous and range from -1.2‰ to +3.7‰. High $\delta^{37}$Cl values are generally correlated with OH-rich zones of replaced apatite, whereas low $\delta^{37}$Cl values are measured in F-rich zones of replaced apatite and in Cl-apatite of probably magmatic origin. Though apatite $\delta^{37}$Cl values follow the general bulk trend, the individual $\delta^{37}$Cl signature seems to reflect the highly localized composition of interfacial fluid at the reaction front.

Our observations suggest that apatite can be used as a fluid probe for F, Br and I to detect a compositional evolution of the fluid, which can be quantified by using experimentally derived partition coefficients. Partitioning of Cl and Cl stable isotopes between highly saline fluids and apatite is complex and likely controlled by more unknown factors than just the Cl concentration.

## Introduction

Halogens (F, Cl, Br and I) are major constituents of all kinds of hydrothermal fluids. Compared to other anions (e.g. $OH^-$, $CO_3^{2-}$, $SO_4^{2-}$), halogen ions have a major impact on petro-physical and chemical properties of solid and liquid phases due to their enhanced complexation capability of dissolved cations (Rapp et al. 2010; Williams-Jones and Heinrich 2005; Tsay et al. 2014). They strongly influence element transport and mobility in fluid media and play a key role in ore-forming processes (Smith et al. 2013; Williams-Jones et al. 2012). As shown by experimental studies, saline fluids enhance the solubility of major silicate phases and lead to a mass transfer of rock forming oxides during metasomatism of crustal and mantle rocks (Newton and Manning 2006; Newton and Manning 2010; Tropper et al. 2013). Also, trace elements like high-field-strength-elements (HFSE) or rare earth elements (REE) which are often considered to be fluid immobile, can be dissolved in halogen-bearing fluids of different composition (John et al. 2008; John et al. 2004; Tropper et al. 2013; Tsay et al. 2014). Although fluid inclusions reveal a direct sample of hydrothermal fluid at pressure-temperature conditions of their entrapment and can be used to extract halogen concentrations of the fluid phase, they can be lacking in some metasomatically altered rock types. Halogen-bearing minerals formed during fluid-rock interaction can provide a probe of halogen concentrations if distribution between mineral and fluid is known. Apart from halogen-bearing amphiboles, mica and scapolite, apatite ($Ca_5(PO_4)_3$[Cl, OH, F]) is a particularly suitable mineral as it incorporates large amounts of halogens in accordance to the halogen activity of the fluid (Kusebauch et al. 2015a; Rasmussen and Mortensen 2013; Yardley 1985; Zhu and Sverjensky 1991; Zhu and Sverjensky 1992). Additionally, apatite reacts sensitively to changing hydrothermal conditions via a coupled dissolution-reprecipitation process in aqueous metasomatic systems (Engvik et al. 2009; Harlov and Forster 2003; Harlov et al. 2002; Jones et al. 2014; Yanagisawa et al. 1999). The newly formed replaced apatite is assumed to be in local equilibrium with the hydrothermal fluid and should, therefore, represent the halogen composition of the fluid. A changing composition of the fluid during apatite replacement will lead to chemical zonation of the replaced apatite with the rim representing an early fluid as it is replaced first and the core being replaced last and therefore, representing a later fluid (e.g., Kusebauch et al. 2015a). In addition to compositional aspects, apatite formed during interaction with aqueous fluid also samples the stable Cl isotopic composition of the hydrothermal system. The Cl isotopic composition (given in standard δ notation, where $\delta^{37}Cl = [((^{37}Cl/^{35}Cl)_{sample} - (^{37}Cl/^{35}Cl)_{SMOC})/(^{37}Cl/^{35}Cl)_{SMOC}]*1000$ and SMOC = Standard Mean Ocean Chloride) for most geologically relevant reservoirs varies between -

8‰ and +3‰ (Barnes and Sharp 2006; John et al. 2010; Sharp et al. 2013). Fractionation of Cl isotopes can be related to processes occurring during fluid-rock interaction (Amundson et al. 2012; Barnes and Cisneros 2012; Kusebauch et al. 2015b; Selverstone and Sharp 2013). The only existing in situ $\delta^{37}Cl$ values of apatite are from studies of Martian and lunar meteorites and range from -4‰ to +9‰ for Martian (Sharp et al. 2014; Shearer et al. 2014) and from +5‰ to +20‰ for lunar apatites. Surprisingly, there are little or no data available on the spatial distribution of halogens and Cl isotopes in apatites from terrestrial samples in general and samples that underwent metasomatism in particular.

To study the behavior of halogens and Cl stable isotopes during interaction of aqueous fluid and apatite, natural samples of hydrothermally altered gabbros from the Kragerø area of Bamble Sector in SE Norway (Fig. 1) were investigated. Recently published halogen and isotope data suggest a local evolution of highly saline fluids during pervasive fluid infiltration along major fluid pathways leading to scapolitisation and amphibolitisation of the gabbroic body at mid crustal P-T conditions (Kusebauch et al. 2015b). Additionally, two different apatite-bearing samples from the well-known Ødegarden verk apatite deposit (Engvik et al. 2009; Harlov et al. 2002), also located in the Bamble Sector, were revisited and analyzed for halogens and Cl stable isotopes.

Here, we compare halogen and Cl stable isotope data of apatite measured in-situ with SIMS with published ex-situ data of bulk and mineral separates to investigate the use of apatite as a fluid probe for halogens.

## Geological setting and sample description

The Bamble Sector is a gneiss terrane of Mesoproterozoic age of prevailing high-grade metamorphism at Sveconorwegian age (1200-980 Ma) (Bingen et al. 2008 and references there in). The Kragerø area of Bamble Sector (Fig. 1) underwent extensive metasomatism by highly saline aqueous and carbonaceous fluids (Engvik et al. 2014; Touret 1985) effecting almost all rock types. In particular, gabbroic rocks, intruded at ~1040 Ma, show large-scale amphibolitisation and scapolitisation caused by the pervasive infiltration of fluids highly enriched in Cl, $CO_2$, Na, K, Mg, P and B (Engvik et al. 2009; Engvik et al. 2011; Kusebauch et al. 2015b). Mid crustal P-T conditions of 600-700°C and 0.2-0.4 GPa are estimated for this metasomatic event (Engvik et al. 2011; Nijland and Touret 2001). Gabbroic bodies are cut by cm- to dm-sized amphibolitic and albitic veins and shear zones into tens of m- to several dm-sized blocks. Starting from these shear zones, the blocks of pristine gabbro are progressively altered by pervasive fluid ingress and show different alteration zones. Fluid inclusions (Nijland and Touret 2001; Touret 1985) and Cl concentrations of amphibole (Kusebauch et al. 2015b) suggest a brinish (~48 wt.% NaCl) composition of the initial fluid, that originates most likely from mobilization of marine sediments and sedimentary pore fluids during orogeny (Bast et al. 2014; Engvik et al. 2011; Kusebauch et al. 2015b).

Two alteration sequences from two different gabbroic bodies (Langøy and Valberg; Fig. 1) were sampled to study fluid-rock interaction under crustal conditions. Both sequences are composed of samples showing different stages of alteration as a function of distance to the shear zone going from pristine gabbro through zones of amphibolitisation and scapolitisation to the shear zone itself. They are described in detail by Kusebauch et al. (2015b). The least altered gabbro of both sequences consists of plagioclase, olivine and clino- and orthopyroxene, the latter three show coronas of pargasitic amphibole. In the amphibolitisation zone olivine and pyroxenes are progressively replaced by Cl-bearing pargasitic amphibole while plagioclase is unaltered. In the scapolitisation zone that follows, plagioclase is replaced by scapolite. Pargasitic amphibole and Ti-rich biotite are other major alteration phases (Kusebauch et al. 2015b). The shear zone consists of monomineralic amphibole, also of pargasitic composition.

The sample from Langøy represents a continuous sequence showing all alteration reactions within a 30x20x10 cm-sized block. In addition to the alteration sequence, a pristine gabbro from the same complex was sampled. Thin sections from the block were sliced perpendicular to the shear zone to provide a profile of increasing distance to the shear zone. Although, the

profile from Valberg is larger (~140 cm), samples show the same alteration sequence according to their distances to the shear zone.

A third set of samples from the Bamble Sector was analyzed to broaden the findings of local fluid-rock interaction concentrated in shear zones to the more regional metasomatic event in the area. For this purpose we reevaluated apatite from samples from the abandoned Apatite mine 'Ødegardens Verk', which was previously studied by Engvik et al. (2009) and Harlov et al. (2002), for halogens and Cl stable isotopes with SIMS. Samples from the Ødegardens Verk include one unaltered gabbro and one scapolitized metagabbro, both of which are described in detail in Engvik et al. (2009).

## Analytical methods

### Electron Microprobe Analyses (EMPA)

We used a JEOL super probe 8900 equipped with 4 wavelength-dispersive spectrometers at the University of Muenster to examine the chemical composition of apatites. Operating conditions for all apatite measurements were 15 kV, 4 nA and spot sizes varied between 2 and 5 µm. To minimize migration of halogens due to extensive electron beam exposure, halogens (F and Cl), CaO and $P_2O_5$ were measured in a first run with low counting times of 10s (Goldoff et al. 2012). All other elements ($K_2O$, $Na_2O$, $SiO_2$, $Ce_2O_3$, MgO) were measured afterwards with counting times ranging from 5-20s. Standardization was done using well established synthetic and natural mineral standards (CaO, $P_2O_5$: Durango apatite; F: synthetic fluoride; Cl: natural tugtupite; $K_2O$: natural sanidine; $Na_2O$: natural jadeite, $Ce_2O_3$: synthetic Ce-phosphate; $SiO_2$: natural hyperstene; MgO: natural olivine). Multiple analyses (n>55) of different apatite standards (including Durango and another F-rich apatite) give a standard deviation for each standard of 1% for CaO, 2% for $P_2O_5$ and ~10% for F and Cl, respectively. Uncertainties for minor elements ($K_2O$, $Na_2O$, $SiO_2$, $Ce_2O_3$, MgO) are in the range of 10% to 20%. Theoretical detection limits for F and Cl are 0.1 and 0.02 wt%, respectively, and for all other elements in the order of 0.02 to 0.06 wt.%. The accuracy of halogen EMPA measurements was checked by using Durango apatite as an unknown. Mean concentrations (n=28) are 3.68 ± 0.27 wt% for F and 0.39 ± 0.05 wt% for Cl, which is in agreement with reported literature data (3.35 ± 0.06 wt% F and 0.46 ± 0.04 wt% Cl; Marks et al. 2012). Structural formula of apatite was calculated for each analyzed apatite on the basis of 26 cations. The OH component ($X_{OH}$=OH/(OH+Cl+F)) was afterwards calculated assuming a perfect solid solution of F, OH and Cl on the anion site and that the difference from the ideal apatite formula on this site is OH.

After finishing quantitative analyses apatite of Langøy samples was mapped for F, Cl, Ca and P and cathodoluminescence (CL) pictures were taken.

### Secondary Ion Mass Spectroscopy (SIMS)

Halogens (i.e., F, Cl, Br, I) and stable Cl isotopes were measured using a CAMECA ims1280 large geometry SIMS instrument at the NORDSIM facility located at the Swedish Museum of Natural History, Stockholm. As different routines for different measurements (i.e., halogen concentrations and Cl stable isotopes) were applied, spots for individual measurements

needed to be set on different positions of the same apatite. This procedure makes a direct comparison of halogen concentrations with Cl isotopic composition of individual spots unfeasible. Nevertheless, positions of individual spots were set close together (in µm distance) and caution was taken to measure in areas with a similar inner structural position and composition as inferred from BSE images and EMPA element maps. In general we measured 3-5 individual spots on 2-3 individual apatite grains from one sample section for Cl isotopes as well as halogen concentrations.

Halogen concentration

Analytical conditions for all measurements closely follow those described by Marks et al. (2012) and Kusebauch et al., (2015a). These were a critically focused ~15µm $^{133}Cs^{+}$ primary beam with ~1.8 nA beam current and 20 kV impact energy (10 kV primary beam, -10 kV secondary beam), low-energy normal-incidence electron flooding to counteract charge build-up on insulating targets, and a mass resolving power (MRP) of 5000 (M/ΔM). Prior to measurement, chosen sites were pre-sputtered for 120s to remove the gold coating over a 25 by 25 µm rastered area and use of a 2500 µm field aperture further minimized surface contamination by restricting the field of view to ca. 22 by 22 µm. Secondary ions were measured either on electron multipliers (< $10^6$ cps) or Faraday cups (>$10^6$ cps) in peak switching mode. Data were acquired over 5 scans with an overall integration time of 120s. At the MRP of 5000, $^{19}F^{-}$, $^{37}Cl^{-}$ and $^{127}I^{-}$ signals were free of molecular interferences; however, neither $^{79}Br^{-}$ nor $^{81}Br^{-}$ can be resolved from $CaCl^{-}$ interferences at MRP < 16000, which cannot be achieved on the ims1280 without significant transmission loss. Hence, a combined $[^{81}Br + {}^{44}Ca^{35}Cl + {}^{46}Ca^{37}Cl]^{-}$ peak was measured and corrected using the intensity of the measured $^{40}Ca^{37}Cl^{-}$ peak together with the natural isotopic abundances of Ca and Cl. All measured peaks were normalized to the matrix $^{40}Ca^{31}P^{-}$ signal and concentrations determined relative to Durango apatite (Kusebauch et al. 2015a). Detection limits are estimated based on an average $^{40}Ca^{31}P$ signal of 300,000 cps and a typical ion counter background of 0.05 cps times three; this yields $6.6*10^{-5}$ µg/g for F, $1.3*10^{-4}$ µg/g for Cl, $3.8*10^{-3}$µg/g for Br and $7.9*10^{-4}$ µg/g for I. Multiple measurements (n=87) of Durango apatite reveal a standard deviation (1σ) of 7% for F, 5% for Cl, 16% for Br and 4% for I, respectively. The uncertainties are in agreement with published data (Marks et al. 2012) for Durango apatite.

220 Chlorine stable isotope measurements

221 $\delta^{37}Cl$ measurements were performed using operating conditions similar to these for halogen
222 measurements (primary beam: 1.3- 2.1 nA, 10 kV, field aperture: 2500, MRP: ~2500, pre
223 sputtering for 120s of 25x25 µm raster). Secondary ions of the stable isotopes $^{35}Cl$ and $^{37}Cl$
224 were measured simultaneously on Faraday cups in multi-collection mode over 40 cycles (4
225 blocks of 10 integrations) with an overall counting time of 160s. Correction for instrumental
226 mass fractionation (IMF) was made using two different apatites (natural Durango and
227 synthetic pure Cl-apatite) of known isotopic composition (measured by stable isotope mass
228 spectrometry of solution from pyrohydrolyses of Durango ($\delta^{37}Cl$=0.5‰) and synthetic Cl-
229 apatite ($\delta^{37}Cl$=2‰)). These reference materials (RM) were regularly interspersed with
230 analyses of the unknown apatites. Multiple measurements of Durango (n=60) and the Cl-
231 apatite RMs (n=70) apatite reveal a relative reproducibility of $\delta^{37}Cl$ of 0.25‰, and 0.15‰,
232 respectively. Internal precision ranges from 0.09 to 0.28‰ for individual measurements. To
233 account for matrix dependent IMF (Godon et al. 2004; Layne et al. 2004), a correction to the
234 measured isotopic ratios was made according to their Cl-concentration assuming a linear
235 concentration dependency of IMF determined from the two different apatite RMs.

236

237

## Results:

### Detailed alteration sequences (Langøy and Valberg)

Apatite is observed in trace abundances in all samples from all localities as anhedral grains varying from 20-300 µm in size (Fig. 2). Apatite from unaltered Langøy and Valberg gabbro is generally zoned and has a Cl-rich zone free of pores and a Cl-poor zone with a large amount of up to µm-sized pores (Fig. 2a-b). Both zones are separated by a sharp interface. Apatite from altered samples is Cl-poor, shows pores and lacks Cl-rich zones (Fig. 2d-e). Although, apatite from altered samples seems to be homogenous when studied by optical microscope and SEM, detailed chemical mapping by EMPA and CL reveals a zonation in F (Fig. 2d and 3). In general, F is enriched in the rims and along cracks of individual apatite grains. These F-rich zones are most prominent in apatite closest to the shear zone and diminish with increasing distance to the shear zone. Areas of high F concentration in apatite coincide with areas of a strong cathodoluminescence.

Although, apatite from the Ødegardens Verk samples shows a similar pattern with Cl-rich and Cl-poor zones (Fig. 2c), they are found in different assemblages. Apatite from the unaltered gabbro sample is a homogenous solid solution of F-apatite and Cl-apatite, whereas apatite from the altered metagabbro and an apatite-phlogopite vein shows Cl-rich and OH-rich zones within the same grain, similar to apatite from unaltered gabbro sample of the Langøy section.

### Cation apatite chemistry (EMPA)

Averaged CaO and $P_2O_5$ concentrations of Cl-rich apatite from pristine gabbro are 53.5 ± 0.7 wt.% and 40.8 ± 0.8 wt.%, respectively (n=36). Cl-poor apatite from altered samples has higher CaO (54.9 ± 0.7 wt.%) and $P_2O_5$ (41.7 ± 0.7 wt.%) concentrations (n=370). Although major components (Ca and P) for Cl-rich and Cl-poor apatite are statistically invariant within the given errors, Cl-rich apatite shows systematically lower concentrations. A similar tendency was found in synthetic Cl-apatite that was replaced by Cl-poor apatite during interaction with aqueous fluids (Kusebauch et al. 2015a). A possible reason for the different Ca and P concentrations of Cl-rich and Cl-poor apatite might be a Ca and P deficiency of pristine magmatic apatite produced during high-temperature crystallization that was erased during replacement with hydrothermal fluid. Averaged Ca/P ratios for all analyzed apatite are 1.66 ± 0.04 and do not vary with anion composition. Minor cations ($K_2O$, $Na_2O$, $SiO_2$, $Ce_2O_3$,

MgO) have generally low concentrations (Table S1) for all measured apatite grains and show no correlation with anion composition or distance to the shear zone.

**F, Cl and OH concentrations (EMPA) of apatite**

Cl-rich apatite from unaltered gabbro of the three locations has Cl concentrations of 6.4 ± 0.4 wt.% for Cl and F concentrations close to or below detection limit (<0.1 wt%) for EMPA. Cl-rich apatite is almost a pure Cl-apatite end member ($X_{Cl}$= 0.95 ± 0.05) with a minor OH component ($X_{OH}$ < 0.1). Cl-poor zones of the same apatite grains range between 0.1 and 0.2 in $X_{Cl}$ (corresponding to 0.5-1.7 wt.% Cl) and show varying F contents depending on the sample locality. Cl-poor apatite from unaltered gabbro from Langøy has no detectable amounts of F (<0.1 wt%) and is, therefore, classified mainly as OH-apatite ($X_{OH}$=0.8-0.9), whereas Cl-poor apatite from unaltered Valberg samples has variable F concentrations. Single measurements show F concentrations up to 1.7 wt.% ($X_F$=0.49). Other individual measurements fall on a trend line between the most F-rich apatite and the most F-poor pristine magmatic apatite (Fig. 4b).

Apatite from the amphibolitisation zone of the Langøy sequence is mainly F-poor OH-apatite ($X_{OH}$=0.8-0.9, $X_{Cl}$=0.1-0.2, $X_F$=0-0.15). Porous zones of apatite from Valberg of the same alteration zone show basically the same composition, also pure Cl-apatite is rarely observed in the amphibolitisation zone (Fig. 4b). With increasing alteration of the gabbro (and decreasing distance to the shear zone) Cl-apatite disappears and porous apatite is enriched in the F-apatite component. Apatite from the scapolititsation zone of both localities is strongly heterogeneous in F and OH components but homogenous in Cl component. Composition ranges from 0 to 0.4 in $X_F$, from 0.4 to 0.9 in $X_{OH}$ and from 0.1 to 0.2 in $X_{Cl}$. Highest F concentrations of up to 1.7 wt.% were measured close to the rim of individual apatite grains or adjacent to cracks. On average, apatite from the altered Valberg samples has lower $X_{Cl}$ than apatite from altered Langøy samples.

**Halogen concentrations and Cl stable isotopes (SIMS) in apatite**

Concentrations of F, Cl, Br and I as well as $\delta^{37}Cl$ of apatite from the Langøy alteration sequence and from the Ødegardens Verk were measured by SIMS in more detail to compare apatite with other halogen-bearing major phases (i.e., amphibole, biotite, and scapolite) from the same sample measured by Kusebauch et al. (2015b). Additionally, SIMS allows the

300 measurement of low concentrations of F. Spots for SIMS analyses were set in a way to
301 measure the different compositional zones within individual apatite crystals as observed by
302 EMPA element maps and CL pictures (Fig. 2 and 3). After analysis individual data points of
303 each sample were grouped into the following zones: 1. Cl-rich and porous free apatite of
304 unaltered gabbro, 2. OH-rich zones, and 3. F-rich zones of apatite from altered samples. To
305 distinguish between zones 2 and 3 we used relative differences in F within individual apatite
306 grains rather than fixed threshold values (see spots in Fig. 3). Although apatites are strongly
307 zoned in halogen composition on a µm-scale and comparison of EMPA and SIMS
308 measurements for F and Cl of the exact same spots is impossible to obtain, halogen
309 concentrations measured with both techniques are in good agreement with each other (Fig. 5).
310 Only Cl concentrations of almost pure Cl-apatite (pore free zones) seem to be overestimated
311 by SIMS as the measured values are higher than the theoretical maximum for pure Cl-apatite
312 (6.8 wt.%) and EMPA measurements. The overestimation might be caused by deviation from
313 an assumed linearity in the concentration working curve, especially considering that Durango
314 apatite used as reference has an order of magnitude lower Cl-concentrations.

315 *Halogens (F, Cl, Br, I)*

316 Fluorine concentrations of Cl-rich apatite from pristine Langøy gabbro samples range
317 between 450 and 915 µg/g (Fig. 6a). In Cl-poor zones of the same apatite grains F is slightly
318 higher and varies from 875 to 1660 µg/g. Bromine values are highest in pore-free apatite
319 (350-1480 µg/g) and lower (117-380µg/g) in the porous zones. A clear trend for I is not
320 observed and concentrations range between 0.2 and 0.5 µg/g for both zones.

321 Although, individual apatite grains from hydrothermally altered Langøy samples are generally
322 heterogeneous, compositional trends can be observed (Fig. 6). As already shown by EMPA
323 measurements, the concentrations of F increase with decreasing distance to the shear zone.
324 Apatite from least-altered samples of the amphibolitization zone has F concentrations of 30-
325 200 µg/g, whereas apatite from highest altered samples has 1000-15000 µg/g (i.e., 0.1-1.5
326 wt.%). When individual spots were grouped according to their relative F contents (i.e., OH-
327 rich apatite and F-rich apatite zone), the trends of increasing concentrations can be observed
328 for the two compositional zones (Fig. 7). Contrastingly, Br shows decreases from 30-85 µg/g
329 in apatite from the least altered samples to 4-25 µg/g in apatite from highly altered samples.
330 Cl concentrations range from 0.4 to 1.8 wt.% without a distinct correlation with distance to
331 the shear zone. Iodine is generally low in all measured apatites and concentrations range from
332 0.15 to 1.2 µg/g.

Apatite from unaltered Ødegardens Verk gabbro is homogeneous and average halogen concentrations are 2.40±0.05 wt% for F, 2.06±0.21 wt.% for Cl, 290±66 µg/g for Br and 0.72±0.03 µg/g for I, respectively, and are in agreement with microprobe data (Engvik et al. 2009). Cl-rich zones of apatite from the metagabbro are also homogenous and have average concentrations of 88±12 µg/g F, 22.9±1.3 µg/g Br and 0.23±0.02 µg/g I. Similar to Cl-rich zones of other Bamble samples, Cl concentrations of pure Cl-apatite are again likely to be overestimated by SIMS measurements. OH-rich zones of the same apatite grain are heterogeneous and values vary between 0.25 and 1.1 wt.% for F, 1.0 and 2.1 wt.% for Cl, 20 and 28 µg/g for Br and 0.25 and 0.48 for I, respectively.

*$\delta^{37}$Cl of apatite*

Cl-rich zones of three individual apatite grains from the unaltered Langøy gabbro sample reveal $\delta^{37}$Cl values in the range of -1.2 to +1.0 ‰ (Fig. 8). Although measurements of Cl-rich zones within individual grains show a homogeneous distribution of $\delta^{37}$Cl values for each grain (Fig. 8), the grains itself differ from each other by 1-2 ‰. Cl-poor apatite of the same samples is heterogeneous and $\delta^{37}$Cl values range from +0.8 to +2.8‰. Cl-poor zones are always higher in $\delta^{37}$Cl than Cl-rich zones of the same grain. Apatite from Langøy samples reflecting different degrees of alteration shows highly variable $\delta^{37}$Cl values that range from -0.7 to +3.7‰ with a slight tendency of higher $\delta^{37}$Cl values towards the shear zone (Fig. 8). Although a simultaneous analysis of $\delta^{37}$Cl values and halogens was not possible, individual spots of $\delta^{37}$Cl can be linked to halogen composition due to their position within the apatite grain determined by elemental mappings (Fig. 3; i.e. OH-rich or F-rich zone). Zones having elevated F concentrations reveal low $\delta^{37}$Cl values and more OH-rich zones show high $\delta^{37}$Cl values (Fig. 8).

Apatite from the unaltered Ødegardens Verk gabbro has $\delta^{37}$Cl value of -0.8 ±0.2 ‰ based on multiple measurement spots on one apatite (n=14). Patchy apatite from the metagabbro sample reveals different $\delta^{37}$Cl values for different zones. Cl-rich apatite has a $\delta^{37}$Cl value of +0.8 ±0.1‰ on average, whereas OH-rich zones of the same apatite show slightly higher values of +1.3 ±0.2 ‰.

## Discussion

### *Apatite replacement reactions*

Apatite is known to react to changes of its surrounding fluid environment via a coupled dissolution-reprecipitation process (Engvik et al. 2009; Kusebauch et al. 2015a; Yanagisawa et al. 1999). In particular, Cl-apatite is affected by replacement as it is the least stable apatite phase in a hydrothermal environment. It has been shown experimentally that Cl-apatite reacts to OH-apatite in the presence of a variety of different geological relevant fluids ranging from high pH fluids (like KOH and NaOH) to neutral NaCl solutions to low pH fluids (HCl-sol) (Kusebauch et al. 2015a; Rendon-Angeles et al. 2000; Yanagisawa et al. 1999). Reaction rates of Cl-apatite replacement are fast (hours to days) and depend mainly on the chemistry of the fluid. In general, replaced apatite (OH- or F- rich) has smaller lattice parameters compared to pristine Cl-apatite and pseudomorphic replacement will lead to the production of pores (Putnis 2002). In turn these pores will affect transport properties as they provide new pathways for the fluid. As the newly formed apatite is precipitating from the fluid during recrystallisation, it is assumed to be in local equilibrium with this fluid and the replaced apatite should, therefore, represent the chemical composition of the fluid. If F is present in the hydrothermal fluid, it will preferentially fractionate into the newly formed apatite (Doherty et al. 2014; Kusebauch et al. 2015a; Zhu and Sverjensky 1991). Once F-rich apatite is formed, it is kinetically hindered from re-equilibrating with a fluid of slightly different composition.

Although metasomatism of the Bamble Sector affected both mafic and felsic rock units and mineral phases therein (e.g., biotite, amphibole, scapolite and feldspars), apatite plays an exceptional role in recording fluid-rock interaction. The different composition of natural apatite from the Bamble area can be explained by the interaction of magmatic apatite with a hydrothermal fluid of changing composition via a coupled dissolution-reprecipitation process. Cl-rich apatite from the unaltered and least altered rock samples of the Langøy and Valberg sequence is interpreted to be of primary magmatic origin (i.e. gabbro) as it shows no pores and individual grains are homogeneous in their halogen composition. Cl-poor zones of the same apatite grains are the result of replacement leading to the production of pores and a sharp interface between Cl-rich and Cl-poor apatite. As the amount of alteration increases towards the shear zone, interaction of pristine apatite with the hydrothermal fluid increases, leading to a complete replacement of magmatic apatite in the altered samples.

Apatite from Ødegardens Verk suggests another possible origin of zoned apatite. Here, magmatic apatite from the most pristine sample is a homogenous solid solution of F- and Cl-apatite (Engvik et al. 2009). Patchy apatite from the metagabbro is then interpreted to originate from interaction of the pristine F-Cl apatite with a high salinity fluid producing a pure Cl-apatite, which in a second process is replaced by OH-rich apatite. Similar to apatite from other shear zone samples from Langøy and Valberg, apatite from Ødegardens Verk is high in F, which suggests a replacement with a fluid similar in composition.

*Apatite as a monitor for halogens in the fluid*

The fluorine case

Fluorine is highly compatible in the apatite structure and experiments reveal distribution coefficients (D) between apatite and NaF-bearing aqueous fluid in the order of 70-300 depending on F concentration in the fluid (Doherty et al. 2014; Kusebauch et al. 2015a). This is one order of magnitude higher than partition coefficients between apatite and melt (Doherty et al. 2014; Mathez and Webster 2005; Webster et al. 2009). The high affinity of F towards apatite will result in a preferred incorporation of F over OH during replacement of precursor apatite. Fluorine-containing fluid that reacts with dry gabbro containing Cl-apatite will become depleted in F during metasomatism due to apatite replacement if sufficient apatite is present. Hereby, F-rich apatite will form first along rims and cracks of precursor Cl-apatite as these are the first parts to react with the fluid (Kusebauch et al. 2015a). Replaced apatite that forms later is in equilibrium with a fluid already depleted in F and is, therefore, relatively OH-rich. This behavior of F during apatite replacement can explain the observed trends in apatite composition with distance to the shear zone (Fig. 6). F-rich zones of individual apatite grains show highest F concentrations close to the shear zone and represent the first replacement product of interaction with the hydrothermal fluid. At this stage, the infiltrating fluid has its highest F concentration. During ongoing pervasive fluid ingress into the reacting rock the fluid gets depleted in F due to ongoing replacement and F partitioning into newly formed apatite. Apatite that is replaced later (i.e., cores of pristine Cl-apatite or apatite far away from the shear zone) has lower F as it is in local equilibrium with an already F-depleted fluid. The evolution of the fluid is in this case recorded by two different observations: 1. by the internal zonation in F of individual apatite grains from different parts of the alteration sequence showing high F at rims and along cracks (Fig. 3) and 2. by the overall higher F concentrations in apatite rims closer the shear zone (Fig. 6).

Another possibility to explain the different zones in F concentration is that two individual fluid pulses of different composition infiltrated the gabbro. The first pulse was characterized by a low F concentration causing the formation of OH-apatite from Cl-apatite, whereas the second pulse was higher in F and formed the F-rich zones of already replaced OH-apatite. Nevertheless, both different pulses would also show an evolution of F concentration of the fluid during ongoing fluid-rock interaction (Fig. 7).

Measured F concentrations of apatite can be used to estimate F concentrations of the hydrothermal fluid that was coexisting with the replaced apatite. Although the partitioning of F between apatite and fluid does not follow Henry´s law behavior as it is a major component in apatite but only a tracer in the fluid, experimental results allow an estimation of the distribution of F between replaced apatite and F bearing fluid (Boyce et al. 2014; Kusebauch et al. 2015a). The distribution can be described as:

$$c^{F}_{fluid} = c^{F}_{apatite} \Big/ D^{F}_{ap/fl} \quad (1)$$

with $D_{ap/fl}^{F}$ being the estimated partition coefficient of F between apatite and fluid and *c* the concentration of F in fluid and apatite. As pointed out by Boyce et al. (2014) the use of halogen partition coefficients in the system melt-apatite is critical and D should be replaced by equilibrium constants ($K_D$) for defined exchange reactions including the activities of all components (i.e., different apatite, OH, F and Cl). Unfortunately, the required activity data do not exist for all components and also their interaction within aqueous solution is poorly constrained and cannot be measured directly from experiments. Therefore, we use partition coefficients derived from experiments as a simplification.

Following empirical correlations from experiments done at the pressure and temperature range of the Bamble metasomatic event (400-700°C and 0.2 GPa; Kusebauch et al. 2015a) with aqueous NaF solutions, replaced apatite with a F concentration of 1.5 wt% (F-rich zones of Langøy apatite) has a D value of 250 and is, therefore, in equilibrium with a fluid having 60 µg/g F. OH-rich apatite with the lowest F concentrations (30-200 µg/g) reveals a F concentration in the replacing fluid of about <1 µg/g. The observed trends of apatite F concentration with distance can be linked to an evolving fluid that had an initial F concentration of ~60 µg/g when it first interacted with the pristine apatite and was depleted to F concentration of less than 1 µg/g due to this interaction. This observation implies that the cores of apatite close the shear zone were replaced at the same time with a fluid of the same composition as the rims of apatite in 15-20 cm distance to the shear zone (Fig. 3).

456 The bromine case

457 Although, replaced apatite is heterogeneous in Br and concentrations can vary over almost an
458 order of magnitude within a single grain, averaged concentrations show decreasing Br
459 towards the shear zone (Fig. 6). If a constant partition of Br between fluid and apatite is
460 assumed, the observed trend implies an evolution of the fluid in its Br concentration. In this
461 case, the Br concentrations of the hydrothermal fluid were highest in the least-altered samples
462 located far away from the shear zone, whereas those close to the shear zone the fluid had less
463 Br. Concentrations of Br in the fluid can be estimated using partition coefficients derived in
464 the same pressure and temperature range estimated for the Bamble metasomatic event
465 (Kusebauch et al. 2015a) by applying following equation:

466 $$c_{fluid}^{Br} = c_{apatite}^{Br} \Big/ D_{ap/fl}^{Br} \quad (2)$$

467 with $D_{ap/fl}^{Br}$ being the experimentally derived partition coefficient between apatite and fluid,
468 $c_{fluid}$ the resulting concentration of Br in the fluid and $c_{apatite}$ the measured concentration of Br
469 in apatite. The use of partition coefficients in the case of Br is justified as Br is a trace element
470 in both, replaced apatite and fluid. By using an experimentally derived partition coefficient
471 (D) of 0.01 for a high salinity fluid (Kusebauch et al. 2015a), Br concentrations of fluid
472 increase from ~1600 µg/g close to the shear zone to ~6500 µg/g in least altered samples. OH-
473 rich apatite from the most pristine sample (metagabbro) was replaced by a fluid with even
474 higher Br concentrations (~15000 µg/g). This fluid is likely to be the last fraction of fluid
475 infiltrating the metagabbro unit and it displayed, therefore, the most evolved fluid.

476 The iodine case

477 Iodine shows fairly constant concentrations throughout the whole alteration sequence and also
478 in magmatic apatite. Although, experiments have shown that I behaves in a similar way to Br
479 during replacement of apatite, a similar trend is not observed in our sample sequence.
480 Nevertheless, using measurements far away from cracks and experimentally derived partition
481 data ($D^{I}_{ap/fl}$ = 0.001) (Kusebauch et al. 2015a) in the same way as for F and Br, I
482 concentrations for the fluid are calculated to be on the order of ~300 µg/g.

483 The chlorine case

484 The calculation of Cl of the hydrothermal fluid in a purely fluid-apatite system is more
485 complex. Based on results of partition experiments in the system apatite-melt-fluid (Doherty
486 et al. 2014; Mathez and Webster 2005; Webster et al. 2009), a linear correlation can be

487 facilitated to estimate melt Cl concentrations from Cl concentrations of coexisting apatite
488 (Boyce et al. 2014; McCubbin et al. 2011). Doherty et al. (2014) show that Cl partitioning
489 between apatite and fluid (in an apatite-fluid-melt system) is depends strongly on melt
490 composition and pressure. Partition coefficients for Cl in such a system vary between 0.1 and
491 1.3. In a reduced system, where only fluid and apatite are present, a simple correlation of
492 apatite composition with fluid composition is not found (Kusebauch et al. 2015a) and apatite
493 composition seems to be a complex function of temperature, pressure, pH, amount and
494 composition of fluid rather than only reliant on its Cl concentration. A reliable estimation of
495 Cl contents in the fluid from an apatite composition alone is, therefore, presently impossible
496 as too many controlling factors are unknown. It is the object of ongoing research.
497 Nevertheless, assuming that halogen partitioning in the apatite-fluid system follows a lattice
498 strain formulation, the partition coefficient for Cl between apatite and fluid is ~2.3
499 (Kusebauch et al. 2015a) and, therefore slightly higher than D values in the apatite-fluid-melt
500 system (Doherty et al. 2014). A calculated Cl concentration for the fluid based on this D value
501 would be in the range of 0.5 wt.%, which is one to two orders of magnitude lower than
502 calculations based on Cl in amphibole suggests (Kusebauch et al. 2015b). The complex
503 partitioning of Cl between fluid and apatite might also explain the large range in Cl
504 composition (0.4-1.8 wt.% by SIMS measurements, Fig. 6) of replaced apatite within a single
505 grain without a distinct correlation with other halogens. Although, a quantification of Cl in the
506 fluid is not possible, the absence of a correlation with distance to the shear zone indicates
507 either a fairly constant fluid composition during its migration through the rocks or a
508 counterbalance of different factors controlling the incorporation of Cl into apatite, e.g. a
509 simultaneous increase of Cl concentration and pH of the fluid will lead to a constant apatite
510 composition.

511

512 *Distribution of chlorine stable isotopes during replacement*

513 The Cl stable isotope system provides a powerful tool to trace interaction of rock with Cl
514 bearing fluids. During fluid-rock interaction, Cl isotopes can be fractionated either by
515 Rayleigh-type or kinetic processes.

516 $\delta^{37}$Cl values of apatite from the Langøy alteration sequence are highly variable and range over
517 almost 4‰. Magmatic Cl-rich apatite precursor zones and replaced F-rich apatite zones have
518 on average 2‰ lower $\delta^{37}$Cl values than those of replaced OH-rich apatite of the same apatite

519 grain (Fig. 8). Additionally, different apatite grains from unaltered gabbro vary between -
520 1.2‰ and +1.0‰ indicating an already existing $\delta^{37}Cl$ variation within the different magmatic
521 Cl-rich apatite grains. This might result from different conditions during their crystallization
522 in a magma chamber. The distribution of Cl stable isotopes can be affected by equilibrium
523 fractionation even at high temperatures (Kusebauch et al. 2015b; Schauble et al. 2003)
524 allowing a Rayleigh fractionation of Cl isotopes in a magma chamber system. This would
525 imply that apatite incorporating Cl early during crystallization would have relatively higher
526 (heavier) $\delta^{37}Cl$ values, whereas apatite forming later has lower (lighter) $\delta^{37}Cl$ values. In the
527 presented sample suite the magmatic apatite with lowest $\delta^{37}Cl$ values also has the lowest F
528 concentration. This argues for either compositional heterogeneity in the magma chamber or a
529 different crystallization time as F is preferentially incorporated in apatite leading to an early
530 relatively F-rich apatite whereas F-poor apatite forms towards the end of crystallization
531 (Boyce, 2014). The different composition of magmatic Cl-rich apatite probably influences the
532 composition of replaced apatite formed from these precursor grains due to its interaction with
533 hydrothermal fluid.

534 F-rich zones of replaced apatite vary between 0 and +2.2‰ in $\delta^{37}Cl$ without a clear trend with
535 distance to the shear zone and values are similar to $\delta^{37}Cl$ values of Cl-rich precursor apatite.
536 As discussed above, the F-rich zones most likely originated early during fluid-rock interaction
537 from a fluid still enriched in F and represent the early alteration products. Assuming a
538 pervasive fluid flow, the amount of fluid present at the beginning of fluid-rock interaction is
539 low. The Cl budget is, therefore, controlled by Cl-bearing minerals (i.e., apatite, amphibole)
540 and their $\delta^{37}Cl$ values. In this case, the $\delta^{37}Cl$ values of F-rich zones of replaced apatite reflect
541 the $\delta^{37}Cl$ values of a rock-dominated system at the beginning of metasomatism: the $\delta^{37}Cl$
542 values are controlled by the magmatic apatite. Due to ongoing fluid infiltration of highly
543 saline fluid (i.e., NaCl/KCl brine), the fluid to rock ratio increases and the Cl budget of the
544 alteration unit is strongly dominated by the infiltrating fluid. Consequently, the higher $\delta^{37}Cl$
545 values of replaced OH-rich apatite represent the $\delta^{37}Cl$ value of the hydrothermal fluid.

546 The observed trend of slightly decreasing $\delta^{37}Cl$ values with increasing distance to the shear
547 zone of OH-rich apatite (Fig. 8) might result either from a decreased fluid to rock ratio far
548 away from the shear zone and, therefore, an increased influence of the lower $\delta^{37}Cl$ of the rock,
549 or an evolution of the Cl isotope ratios of the fluid towards lower values. Kusebauch et al.
550 (2015b) interpret decreasing $\delta^{37}Cl$ values of amphiboles and bulk samples from the same
551 alteration sequence to be the result of Rayleigh fractionation of Cl isotopes due to the

552 consumption of heavier Cl and incorporation into rock-forming Cl bearing phases (i.e.,
553 amphibole, biotite and scapolite). This results in an evolving fluid which changes its $\delta^{37}Cl$
554 value during pervasive fluid flow and interaction with unaltered gabbro.

555 A second possible explanation would be the influence of different fluids leading to different
556 replacement events. Assuming two different fluid pulses or events, the different $\delta^{37}Cl$ values
557 of F-rich and F-poor zones (Fig. 8b) would represent the Cl isotope composition of individual
558 fluids. In this case the F-poor fluid (first fluid) will have a high $\delta^{37}Cl$ value of ~ +3.5‰ and
559 the F-rich fluid (second fluid) will have a lower $\delta^{37}Cl$ value of ~ +1‰. In this case all other
560 $\delta^{37}Cl$ values would result from mixing between the different fluids and the magmatic values.
561 Apart from apatite, no other mineral present in the alteration sequence shows indications of
562 two fluid events. All isotopic and compositional features of amphibole and bulk can be
563 explained by evolution of the fluid phase of a single event (Kusebauch et al. 2015b).
564 Therefore, we interpret the different zones observed in F concentration and $\delta^{37}Cl$ of replaced
565 apatite as the result of the same fluid event and related evolution due to fluid-rock interaction.

566 Although absolute $\delta^{37}Cl$ values of apatite from the Ødegardens Verk are different from values
567 of Langøy apatite, they display a similar pattern in $\delta^{37}Cl$ during replacement. Magmatic
568 apatite, in this case a solid solution of F-apatite and Cl-apatite, has the lowest $\delta^{37}Cl$ value of -
569 0.8 ±0.2‰, which is similar to the lowest $\delta^{37}Cl$ values of magmatic apatite from Langøy. If
570 almost pure Cl-apatite is already a product of fluid-rock interaction, as suggested by Engvik et
571 al. (2009), their $\delta^{37}Cl$ value of +0.8 ±0.1‰ represents the influence of Cl from an extremely
572 saline hydrothermal fluid. OH-rich apatite with a $\delta^{37}Cl$ value of +1.3 ±0.2‰ is most
573 representative for the fluid as it originates from replacement of Cl-rich apatite and should,
574 therefore, be in equilibrium with fluid. The observations made in the Ødegardens Verk
575 samples suggest interaction of a fluid with high $\delta^{37}Cl$ and magmatic apatite with low $\delta^{37}Cl$ for
576 the whole area.

577 Although spatially resolved SIMS measurements provide an additional tool to study stable Cl
578 isotopes, the interpretation of the data is complicated. It seems that single apatite grains are
579 very heterogeneous and incorporation of different Cl isotopes into apatite is probably affected
580 by various competing fractionation and mixing processes. Non-spatially resolved methods to
581 measure Cl stable isotopes will not suffer from these very local heterogeneities and will show
582 processes on a larger scale.

583 *Correlations of halogen data from apatite with bulk and silicate mineral separates*

584 Fluid-rock interaction in the Bamble Sector leads not only to replacement of apatite but also
585 replacement of primary magmatic halogen-free olivine, pyroxene and plagioclase by halogen-
586 bearing alteration minerals amphibole, biotite and scapolite. Halogens of mineral separates as
587 well as bulk samples from the same alteration sequence were measured by ion
588 chromatography (for F) and ICP-MS of pyrohydrolysis solutions (for Cl, Br and I)
589 (Kusebauch et al. 2015b). Halogen concentrations of alteration silicates and bulk samples
590 reveal following major results: 1. generally low F concentrations (< 300 µg/g) in bulk samples
591 and minerals; 2. very high Cl and Br bulk concentrations (up to 1.1 wt.% Cl and ~30 µg/g Br)
592 close to the shear zone and decreasing but relatively high concentrations (0.4-0.5 wt.% Cl and
593 ~10 µg/g Br) towards unaltered gabbro; 3. constant I for all bulk rock and mineral separates;
594 4. increasing Cl and Br concentrations of amphibole with increasing distance to the shear
595 zone; and 5. decreasing $\delta^{37}Cl$ values towards unaltered gabbro. These findings suggest an
596 intensive interaction of gabbro with a pervasive infiltrating highly saline fluid of evolving
597 halogen composition (Engvik et al. 2011; Kusebauch et al. 2015b). In this context apatite
598 provides an additional probe for halogens as it replaces in accordance to an evolving fluid.

599 Fluorine

600 Apart from apatite biotite, which is stable close to the shear zone but not throughout the whole
601 alteration sequence, is another potential host for F. However, F concentrations of biotite are
602 low (130-340 µg/g) indicating low F concentrations of the hydrothermal fluid also during the
603 formation of biotite (Kusebauch et al. 2015b). Amphibole and scapolite that formed during
604 fluid-rock interaction incorporates F in a range of 100-350 µg/g and 40-100 µg/g, respectively
605 and show highest F concentrations close to the shear zone similar to apatite.

606 Chlorine

607 Although, Cl in amphibole shows an increasing concentration trend with decreasing
608 alteration, which is related to an increase in Cl concentration of the infiltrating fluid due to
609 desiccation as it reacts with unaltered rock, Cl contents in apatite are constant throughout the
610 same section. Nevertheless, apatite should record significant changes of Cl concentration in
611 the fluid similar to amphibole if partitioning controlling factors (i.e., pH, T, P, cation
612 concentration) are constant for all samples. The absence of a compositional trend is, therefore,
613 either the result of simultaneously changing factors that work opposite to each other (e.g., pH
614 and cation concentration) or the changes of Cl concentration in the fluid are too small to be
615 reflected in the apatite composition. The latter explanation seems to be more likely as the

calculated composition of the fluid based on Cl in amphibole (see Kusebauch et al. 2015a for calculation) changes during infiltration from 48 wt.% NaCl ($X_{NaCl}$=0.22) close to the shear zone to 73 wt.% ($X_{NaCl}$=0.45) in the least altered samples. Additionally, apatite seems to be replaced faster than silicates and might be formed prior to the desiccation-related Cl concentration changes of the fluid.

Bromine and Iodine

Bromine behaves differently as it is a trace element in the fluid as well as in alteration minerals. The trend of increasing Br with decreasing alteration produced by a desiccated fluid is observed in apatite as well as in amphibole. Combination of Br, I and F data for the fluid from this study with Cl data from Kusebauch et al. (2015b) enables the calculation of representative halogen ratios for the infiltrating fluid. The Cl concentration of the unevolved fluid is 29.1 wt.% (based on a salinity of 48 wt.%) as calculated from amphibole data, Br concentration of the same fluid is about 1600 µg/g. I is about 300µg/g and F concentration is around 60 µg/g as calculated from apatite composition. Therefore, the Br/Cl, I/Cl and F/Cl are $5.5*10^{-3}$, $1*10^{-3}$ and $0.2*10^{-3}$, respectively. The calculated Br/Cl and I/Cl ratios for the initial fluid are in good agreement with the estimated ratios by Kusebauch et al. (2015b) of $>3*10^{-3}$ for Br/Cl and $>0.025*10^{-3}$ for I/Cl and supports their interpretation of the fluid being derived from marine pore fluids and marine sediments rather than from remobilization of evaporites. Also, the low F/Cl ratio argues for an origin related to a marine environment of the Bamble fluids as other fluid reservoirs (i.e., magmatic fluids, altered crust, mantle) have orders of magnitude higher F/Cl ratios (John et al. 2011).

Cl isotopes

The Cl isotopic values of bulk-rock and mineral separates (i.e., amphibole, biotite and scapolite) of the Langøy and Valberg alteration sequence vary between -0.7 and +1.0‰, and -1.8 and +1.2‰, respectively. In general, low $\delta^{37}$Cl values are found in less altered samples, whereas higher $\delta^{37}$Cl values are mainly observed in highly altered samples. It is important to state that $\delta^{37}$Cl of bulk and silicates were measured by isotope ratio mass spectrometer analysis of a pyrohydrolyses solution containing extracted Cl from powdered samples (Barnes and Sharp 2006; Kusebauch et al. 2015b). For this method a certain amount of either bulk rock powder or powder of mineral separates needs to be prepared. Consequently, all local heterogeneities in $\delta^{37}$Cl within individual grains are removed and an average $\delta^{37}$Cl value is measured. Spatially resolved analysis of apatite $\delta^{37}$Cl by SIMS reveals strong heterogeneities

within individual grains as well as between different grains of the same sample. Although, lowest $\delta^{37}Cl$ values for apatite of each sample fall in the range of values measured for bulk rock and mineral separates, the majority of $\delta^{37}Cl$ values are 1-2‰ higher.

As discussed before, one possible process that might produce heterogeneities is a variable mixing of Cl from the different reservoirs, i.e., fluids and pristine magmatic apatite, during the replacement of apatite. Isotope fractionation processes can also lead to a locally heterogeneous distribution of Cl isotopes in replaced apatite. Diffusion experiments (Eggenkamp and Coleman 2009) show that kinetic fractionation is a potential process to change the Cl isotopic signal by 3-4‰ due to different diffusion coefficients of the two isotopes. Also, equilibrium fractionation of Cl isotopes due different bonding of Cl in molecules and crystals can cause variations of $\delta^{37}Cl$ values between different Cl species (Gleeson and Smith 2009; Kusebauch et al. 2015b; Schauble et al. 2003; Sharp et al. 2010). If Cl atoms are exchanged between different types of species on a larger scale (i.e., incorporation of Cl into minerals from a fluid, changing from solid state to aqueous to gaseous) Rayleigh fractionation will become an additional factor to influence the Cl isotopic composition of a system. Unfortunately, equilibrium fractionation data are lacking, but calculations based on ab-initio and lattice dynamics modelling (Schauble et al. 2003) suggest a fractionation in the order of 1.5‰ between Cl-metal complexes and non-bonding Cl even at temperatures of 300°C. This implies that apatite crystallizing from a hydrothermal fluid is likely to have a 1.5‰ higher $\delta^{37}Cl$ value than the fluid, which might account for some of the observed variation. Replacement via a coupled dissolution-reprecipitation process always requires an interfacial fluid, which can be highly variable on a µm scale in composition but also in its physico-chemical properties and heterogeneities of this fluid might be imprinted in the replacement product.

## Conclusions: Ability of applying apatite as a halogen probe

Apatite reacts via a coupled dissolution-reprecipitation process during fluid-rock interaction and incorporates halogens as a function of fluid chemistry. Halogen composition of apatite from metagabbros of the Bamble Sector (SE Norway) reveals information about the composition and history of hydrothermal fluid processes during a regional metasomatic event. Although, replaced apatite is heterogeneous in halogen and Cl isotope composition, distinctive trends can be observed suggesting a compositional evolution of fluid during fluid-

rock interaction. Halogen concentrations of the fluid were estimated using experimentally derived partition data between fluid and apatite at the P-T conditions of the Bamble metasomatic event. Relatively high F concentrations of replaced apatite adjacent to the shear zone indicate an infiltration of fluid having ~60 µg/g dissolved F. During pervasive fluid flow and ongoing apatite replacement, F is preferentially incorporated into apatite and depleted in the fluid to very low concentrations (>1 µg/g). Conversely, calculated Br concentrations of the fluid increase from ~1600 µg/g to ~6500 µg/g during evolution of the fluid, which is in agreement with observations of amphibole compositions of the same samples. Calculated I concentrations of the fluid are constant in the order of 300 µg/g. Using apatite to probe Cl concentrations and Cl stable isotopes has limitations. Cl concentrations of replaced apatite cannot be directly related to the Cl concentrations of the fluid and trends in Cl composition of amphibole (Kusebauch et al. 2015b) are not confirmed by the apatite composition, which might be related to the high Cl concentrations of the brine-like fluids. Apart from Cl, apatite can be used as a probe for halogens. In particular, spatially resolved F, Br and I data of replaced apatite helps to understand the compositional evolution of a hydrothermal fluid during interaction with unaltered gabbro by pervasive fluid flow.

Although, $\delta^{37}$Cl values of different apatites from the Bamble Sector are heterogeneous and vary between individual grains from the same sample as well as within a single apatite grain in the order of 1-3‰, they show some patterns in their halogen composition. The most pristine magmatic Cl-rich apatite has lowest $\delta^{37}$Cl values (-1.2 to +1.0‰), replaced F-rich apatite has slightly higher $\delta^{37}$Cl values (-0.7 to 1.5‰) and replaced OH-rich apatite shows $\delta^{37}$Cl values of +0.6 to +3.7‰. It seems that this increase reflects the compositional change of the progressively infiltrating fluid reacting locally with apatite. However, interpreting $\delta^{37}$Cl values in the context of fluid history and evolution, especially from apatite alone, is complicated as only little is known about mixing and fractionation processes of the Cl isotopic system during incorporation of Cl from a fluid into minerals.

## References


Amundson R, Barnes JD, Ewing S, Heimsath A, Chong G (2012) The stable isotope composition of halite and sulfate of hyperarid soils and its relation to aqueous transport. Geochim Cosmochim Acta 99:271-286

Barnes JD, Cisneros M (2012) Mineralogical control on the chlorine isotope composition of altered oceanic crust. Chem Geol 326:51-60 doi:DOI 10.1016/j.chemgeo.2012.07.022

Barnes JD, Sharp ZD (2006) A chlorine isotope study of DSDP/ODP serpentinized ultramafic rocks: Insights into the serpentinization process. Chem Geol 228:246-265

Bast R et al. (2014) Boron isotopes in tourmaline as a tracer of metasomatic processes in the Bamble sector of Southern Norway. Contrib Mineral Petr 168:1069

Bingen B, Davis WJ, Hamilton MA, Engvik AK, Stein HJ, Skar O, Nordgulen O (2008) Geochronology of high-grade metamorphism in the Sveconorwegian belt, S. Norway: U-Pb, Th-Pb and Re-Os data. Norw J Geol 88:13-42

Boyce JW, Tomlinson SM, McCubbin FM, Greenwood JP, Treiman AH (2014) The Lunar Apatite Paradox. Science 344:400-402 doi:DOI 10.1126/science.1250398

Doherty AL, Webster JD, Goldoff BA, Piccoli PM (2014) Partitioning behavior of chlorine and fluorine in felsic melt–fluid(s)–apatite systems at 50MPa and 850–950°C. Chem Geol 384:94-109 doi:http://dx.doi.org/10.1016/j.chemgeo.2014.06.023

Eggenkamp HGM, Coleman ML (2009) The effect of aqueous diffusion on the fractionation of chlorine and bromine stable isotopes. Geochim Cosmochim Acta 73:3539-3548 doi:DOI 10.1016/j.gca.2009.03.036

Engvik AK, Golla-Schindler U, Berndt J, Austrheim H, Putnis A (2009) Intragranular replacement of chlorapatite by hydroxy-fluor-apatite during metasomatism. Lithos 112:236-246

Engvik AK, Ihlen PM, Austrheim H (2014) Characterisation of Na-metasomatism in the Sveconorwegian Bamble Sector of South Norway. Geoscience Frontiers 5:659-672 doi:http://dx.doi.org/10.1016/j.gsf.2014.03.008

Engvik AK et al. (2011) Metasomatism of gabbro - mineral replacement and element mobilization during the Sveconorwegian metamorphic event. J Metamorph Geol 29:399-423

Gleeson SA, Smith MP (2009) The sources and evolution of mineralising fluids in iron oxide-copper-gold systems, Norrbotten, Sweden: Constraints from Br/Cl ratios and stable Cl isotopes of fluid inclusion leachates. Geochim Cosmochim Acta 73:5658-5672 doi:DOI 10.1016/j.gca.2009.06.005

Godon A, Webster JD, Layne GD, Pineau F (2004) Secondary ion mass spectrometry for the determination of delta Cl-37 Part II. Intercalibration of SIMS and IRMS for aluminosilicate glasses. Chem Geol 207:291-303 doi:DOI 10.1016/j.chemgeo.2004.04.003

Goldoff B, Webster JD, Harlov DE (2012) Characterization of fluor-chlorapatites by electron probe microanalysis with a focus on time-dependent intensity variation of halogens. Am Mineral 97:1103-1115 doi:Doi 10.2138/Am.2012.3812

Harlov DE, Forster HJ (2003) Fluid-induced nucleation of (Y+REE)-phosphate minerals within apatite: Nature and experiment. Part II. Fluorapatite. Am Mineral 88:1209-1229

Harlov DE, Forster HJ, Nijland TG (2002) Fluid-induced nucleation of (Y+REE)-phosphate minerals within apatite: Nature and experiment. Part I. Chlorapatite. Am Mineral 87:245-261

John T, Klemd R, Gao J, Garbe-Schonberg CD (2008) Trace-element mobilization in slabs due to non steady-state fluid-rock interaction: Constraints from an eclogite-facies transport vein in blueschist (Tianshan, China). Lithos 103:1-24 doi:DOI 10.1016/j.lithos.2007.09.005

John T, Layne GD, Haase KM, Barnes JD (2010) Chlorine isotope evidence for crustal recycling into the Earth's mantle. Earth Planet Sc Lett 298:175-182

John T, Scherer EE, Haase K, Schenk V (2004) Trace element fractionation during fluid-induced eclogitization in a subducting slab: trace element and Lu-Hf-Sm-Nd isotope systematics. Earth Planet Sc Lett 227:441-456

John T, Scambelluri M, Frische M, Barnes JD, Bach W (2011) Dehydration of subducting serpentinite: Implications for halogen mobility in subduction zones and the deep halogen cycle. Earth Planet Sc Lett 308:65–76.

Jones RH, McCubbin FM, Dreeland L, Guan Y, Burger PV, Shearer CK (2014) Phosphate minerals in LL chondrites: A record of the action of fluids during metamorphism on ordinary chondrite parent bodies. Geochim Cosmochim Acta 132:120-140 doi:http://dx.doi.org/10.1016/j.gca.2014.01.027

Kusebauch C, John T, Whitehouse MJ, Klemme S, Putnis A (2015a) Distribution of Halogens between Fluid and Apatite during fluid-mediated replacement processes. Geochim Cosmochim Acta - accepted

Kusebauch C, John T, Barnes J, Klügel A, Austrheim H (2015b) Halogen element and stable chlorine isotope fractionation caused by fluid-rock interaction (Bamble sector SE Norway). J Petrol 56:299-324

Layne GD, Godon A, Webster JD, Bach W (2004) Secondary ion mass spectrometry for the determination of delta Cl-37 Part I. Ion microprobe analysis of glasses and fluids. Chem Geol 207:277-289 doi:DOI 10.1016/j.chemgeo.2004.04.002

Marks MAW et al. (2012) The volatile inventory (F, Cl, Br, S, C) of magmatic apatite: An integrated analytical approach. Chem Geol 291:241-255

Mathez EA, Webster JD (2005) Partitioning behavior of chlorine and fluorine in the system apatite-silicate melt-fluid. Geochim Cosmochim Acta 69:1275-1286

McCubbin FM et al. (2011) Fluorine and chlorine abundances in lunar apatite: Implications for heterogeneous distributions of magmatic volatiles in the lunar interior. Geochim Cosmochim Acta 75:5073-5093 doi:DOI 10.1016/j.gca.2011.06.017

Newton RC, Manning CE (2006) Solubilities of corundum, wollastonite and quartz in H2O-NaCl solutions at 800 degrees C and 10 kbar: Interaction of simple minerals with brines at high pressure and temperature. Geochim Cosmochim Acta 70:5571-5582 doi:DOI 10.1016/j.gca.2006.08.012

Newton RC, Manning CE (2010) Role of saline fluids in deep-crustal and upper-mantle metasomatism: insights from experimental studies. Geofluids 10:58-72 doi:DOI 10.1111/j.1468-8123.2009.00275.x

Nijland TG, Touret JLR (2001) Replacement of graphic pegmatite by graphic albite-actinolite-clinopyroxene intergrowths (Mjavatn, southern Norway). Eur J Mineral 13:41-50

Putnis A (2002) Mineral replacement reactions: from macroscopic observations to microscopic mechanisms. Mineral Mag 66:689-708

Rapp JF, Klemme S, Butler IB, Harley SL (2010) Extremely high solubility of rutile in chloride and fluoride-bearing metamorphic fluids: An experimental investigation. Geology 38:323-326 doi:Doi 10.1130/G30753.1

Rasmussen KL, Mortensen JK (2013) Magmatic petrogenesis and the evolution of (F:Cl:OH) fluid composition in barren and tungsten skarn-associated plutons using apatite and biotite compositions: Case studies from the northern Canadian Cordillera. Ore Geol Rev 50:118-142 doi:DOI 10.1016/j.oregeorev.2012.09.006

Rendon-Angeles JC, Yanagisawa K, Ishizawa N, Oishi S (2000) Effect of metal ions of chlorapatites on the topotaxial replacement by hydroxyapatite under hydrothermal conditions. J Solid State Chem 154:569-578

Schauble EA, Rossman GR, Taylor HP (2003) Theoretical estimates of equilibrium chlorine-isotope fractionations. Geochim Cosmochim Acta 67:3267-3281

Selverstone J, Sharp ZD (2013) Chlorine isotope constraints on fluid-rock interactions during subduction and exhumation of the Zermatt-Saas ophiolite. Geochemistry, Geophysics, Geosystems 14:4370-4391 doi:10.1002/ggge.20269

Sharp Z, Shearer CK, Burger PV, Agee C, McKeegan KD (2014) The unique Chlorine Isotope composition of Mars: Implications for planetary formation and differentiation. Paper presented at the 45th LPSC Conference, Houston,

Sharp ZD, Barnes JD, Fischer TP, Halick M (2010) An experimental determination of chlorine isotope fractionation in acid systems and applications to volcanic fumaroles. Geochim Cosmochim Ac 74:264-273 doi:DOI 10.1016/j.gca.2009.09.032

Sharp ZD, Mercer JA, Jones RH, Brearley AJ, Selverstone J, Bekker A, Stachel T (2013) The chlorine isotope composition of chondrites and Earth. Geochim Cosmochim Acta 107:189-204 doi:DOI 10.1016/j.gca.2013.01.003

Shearer CK, Sharp Z, McKeegan KD, Burger PV, McCubbin FM (2014) Chlorine isotopic composition of martian meteorites. Implications for the composition of the martian crust and mantle, their interactions, and magmatic processes. Paper presented at the 45th LPSC Conference, Houston,

Smith MP, Gleeson SA, Yardley BWD (2013) Hydrothermal fluid evolution and metal transport in the Kiruna District, Sweden: Contrasting metal behaviour in aqueous and aqueous-carbonic brines. Geochim Cosmochim Acta 102:89-112

Touret J (1985) Fluid Regime in Southern Norway: The Record of Fluid Inclusions. In: Tobi ACaT, J. (ed) The Deep Proterozoic Crust in the North Atlantic Provinces. D.Reidel, pp 517-549

Tropper P, Manning CE, Harlov DE (2013) Experimental determination of CePO4 and YPO4 solubilities in H2O-NaF at 800 degrees C and 1 GPa: implications for rare earth element transport in high-grade metamorphic fluids. Geofluids 13:372-380 doi:Doi 10.1111/Gfl.12031

Tsay A, Zajacz Z, Sanchez-Valle C (2014) Efficient mobilization and fractionation of rare-earth elements by aqueous fluids upon slab dehydration. Earth Planet Sc Lett 398:101-112 doi:http://dx.doi.org/10.1016/j.epsl.2014.04.042

Webster JD, Tappen CM, Mandeville CW (2009) Partitioning behavior of chlorine and fluorine in the system apatite-melt-fluid. II: Felsic silicate systems at 200 MPa. Geochim Cosmochim Acta 73:559-581

Williams-Jones AE, Heinrich CA (2005) 100th Anniversary special paper: Vapor transport of metals and the formation of magmatic-hydrothermal ore deposits. Econ Geol 100:1287-1312 doi:Doi 10.2113/100.7.1287

Williams-Jones AE, Migdisov AA, Samson IM (2012) Hydrothermal Mobilisation of the Rare Earth Elements - a Tale of "Ceria" and "Yttria". Elements 8:355-360 doi:DOI 10.2113/gselements.8.5.355

Yanagisawa K, Rendon-Angeles JC, Ishizawa N, Oishi S (1999) Topotaxial replacement of chlorapatite by hydroxyapatite during hydrothermal ion exchange. Am Mineral 84:1861-1869

Yardley BWD (1985) Apatite Composition and the Fugacities of Hf and Hcl in Metamorphic Fluids. Mineral Mag 49:77-79

Zhu C, Sverjensky DA (1991) Partitioning of F-Cl-Oh between Minerals and Hydrothermal Fluids. Geochim Cosmochim Acta 55:1837-1858

Zhu C, Sverjensky DA (1992) F-Cl-Oh Partitioning between Biotite and Apatite. Geochim Cosmochim Acta 56:3435-3467

Figures:

Fig. 1: Geological map of the Kragerø area in the north eastern part of the Bamble Sector showing the sample sites (stars) near Kragerø (Valberg), at Langøy and Ødegardens Verk (from Geological Survey of Norway bedrock database).

Fig. 2: Back scatter electron (BSE) and cathodoluminescence (CL) images of apatite from Bamble: a) patchy Cl-rich and OH-rich apatite from Langøy gabbro, b) apatite from slightly altered Valberg metagabbro showing a pore-free Cl-rich apatite core surrounded by porous OH-rich apatite rim, c) patchy apatite from Ødegardens Verk metagabbro (picture from Engvik et al. 2009), d) OH-rich apatite from amphibolitized metagabbro, e) OH-rich apatite from scapolitized Langøy metagabbro, f) CL image of same apatite showing CL active zones along cracks.

Fig. 3: Langøy alteration sequence (~30 cm in size) going from the shear zone (upper part) down to the pristine gabbro (PG) sample (lower part). Alteration is strongest close to the shear zone and decreases towards PG; a) thin sections scans; b) Fluorine and Cl maps of different apatite grains in accordance to their position within the alteration sequence (spots mark individual SIMS measurements of halogen concentrations (green) and $\delta^{37}$Cl (red)).

Fig. 4: Ternary representation (i.e., $X_F$, $X_{OH}$, $X_{Cl}$) of apatite composition for Langøy (left) and Valberg (right) sample sequence calculated on the base of EMPA measurements.

Fig. 5: Comparison of Cl (a) and F (b) concentrations measured by EMPA and SIMS of individual apatite grains, error bars: S.D. values of multiple spots in identical zones within a single grain.

Fig. 6: Halogen concentrations (by SIMS) of apatite in accordance to the distance to the shear zone; each point represents an individual analytical spot; same color = individual grain of the same sample, analytical uncertainty is smaller or equal to symbol size.

Fig. 7: Boxplots of halogen concentration for each sample; blue: Cl-rich apatite of unaltered gabbro sample, red: F-rich zone of replaced apatite, green: OH-rich zone of replaced apatite.

Fig. 8: $\delta^{37}$Cl values of individual apatite grains as a function of their distance to the shear zone; same color coding as in Fig. 6 and Fig. 7.

879

880

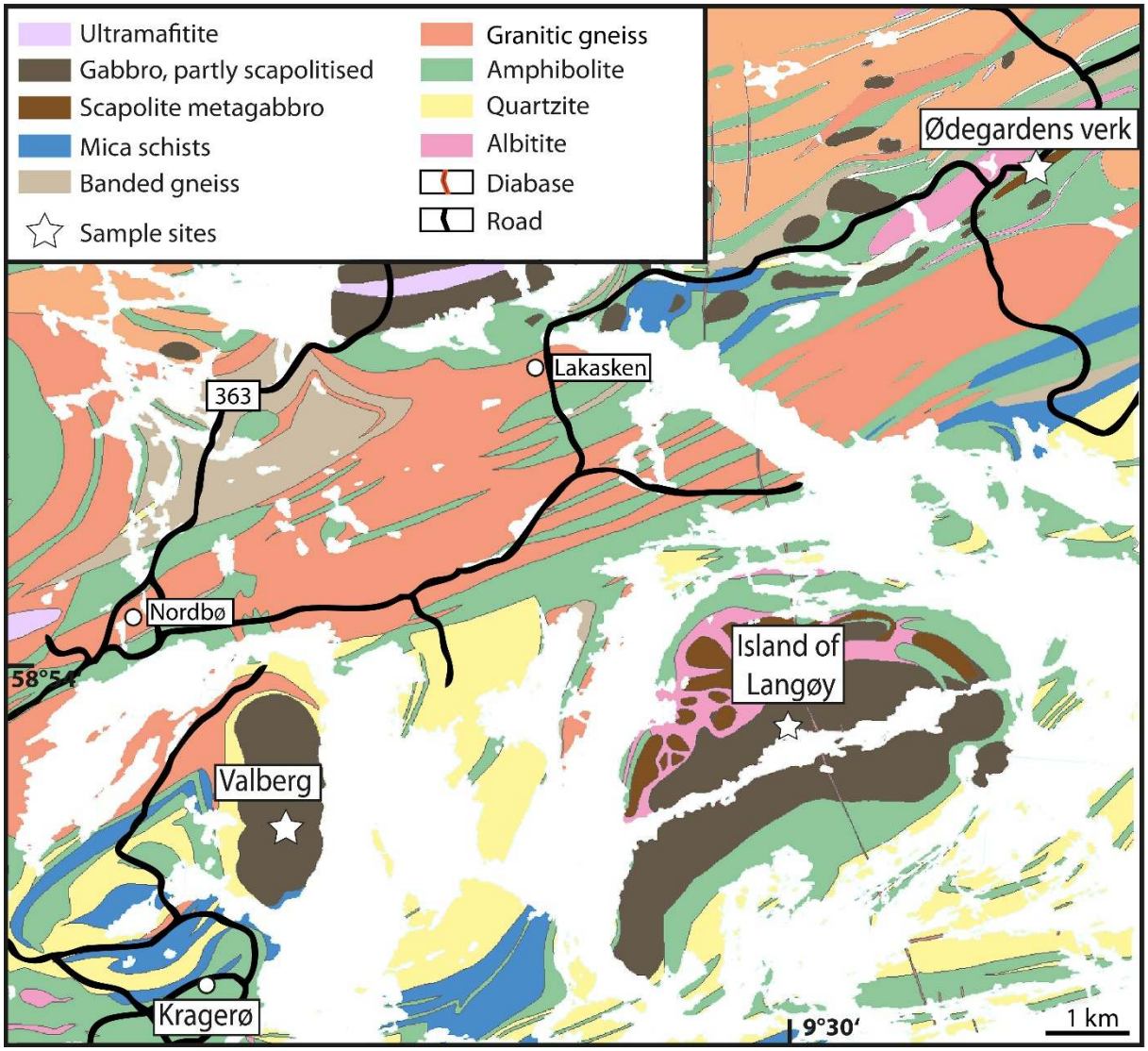


881

882 Fig. 1

883

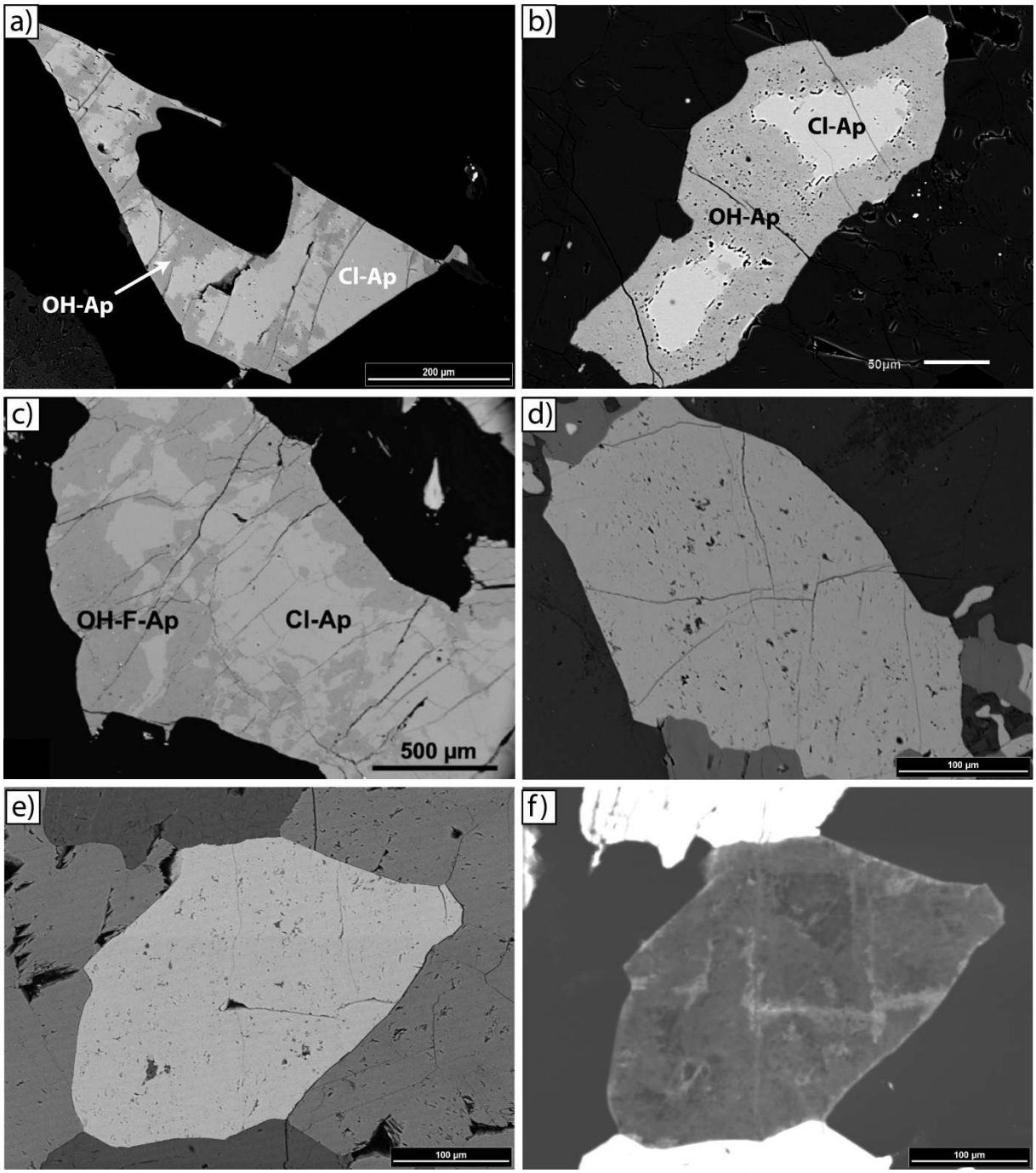


884

885 Fig. 2

886

887

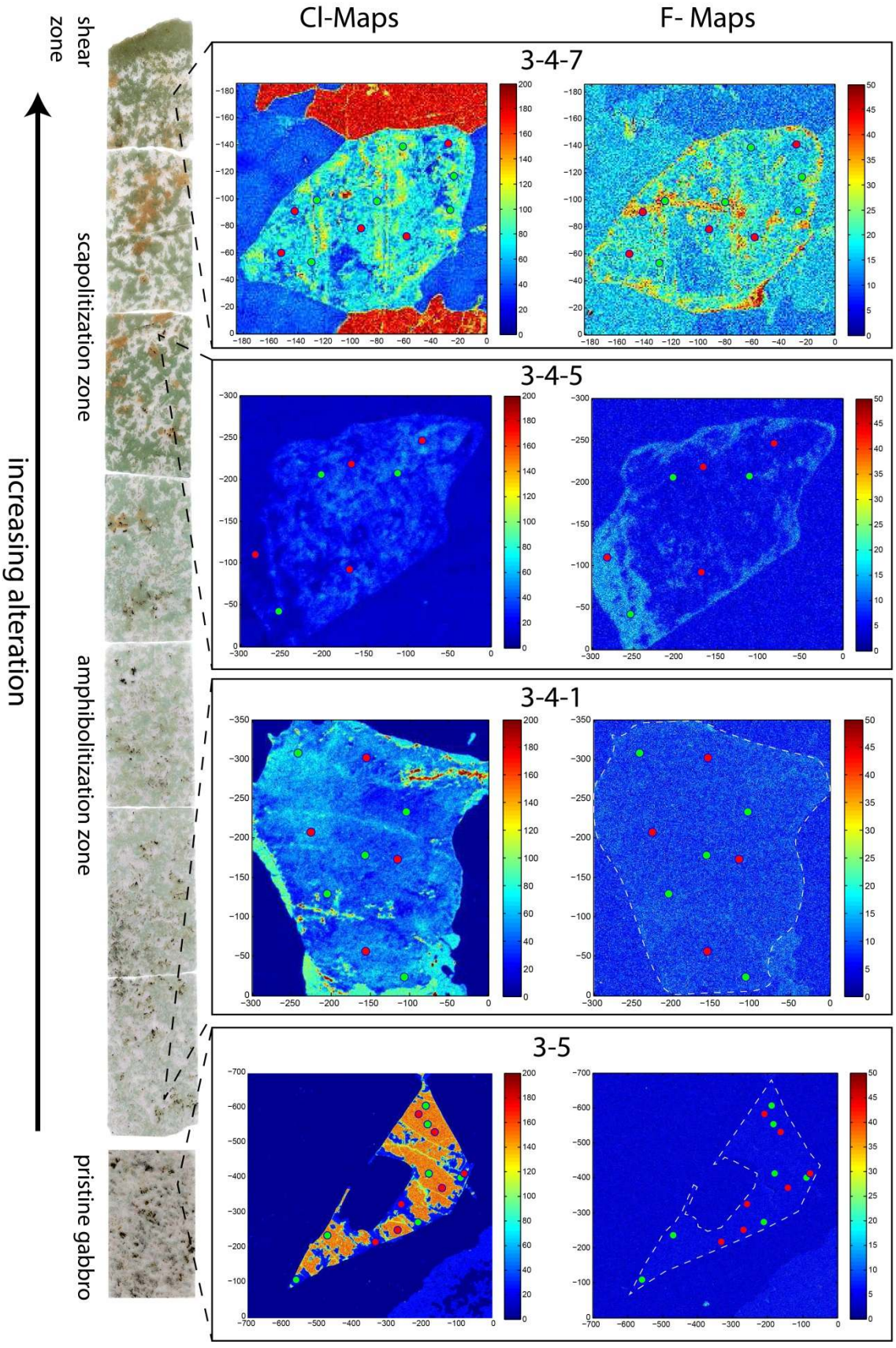
Cl-Maps
F- Maps
3-4-7
3-4-5
3-4-1
3-5
shear zone
scapolitization zone
amphibolitization zone
pristine gabbro
increasing alteration

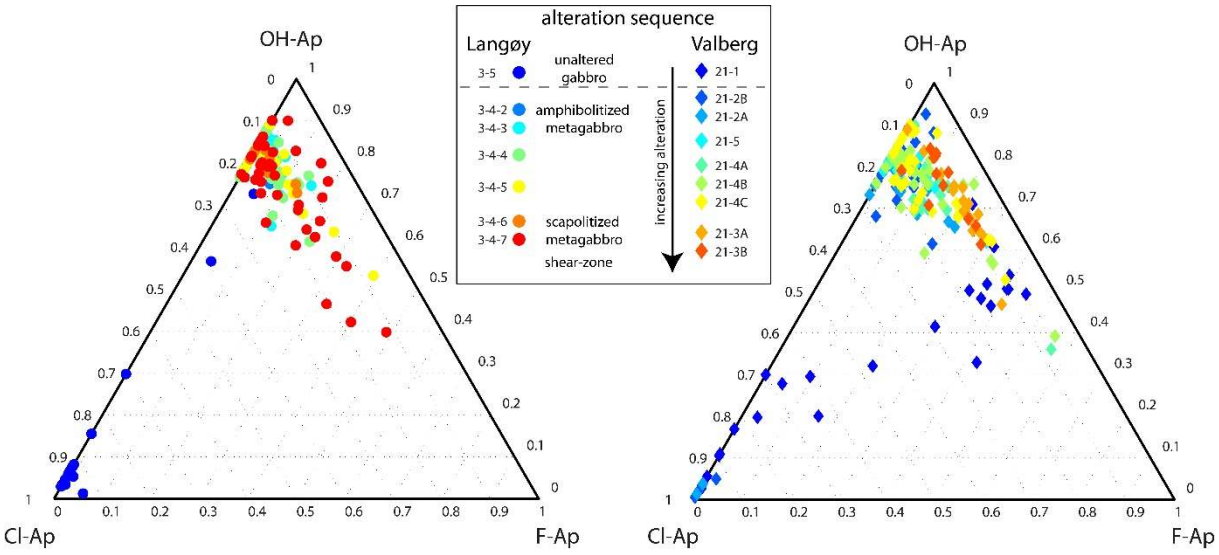


889

890 Fig. 4

891

892

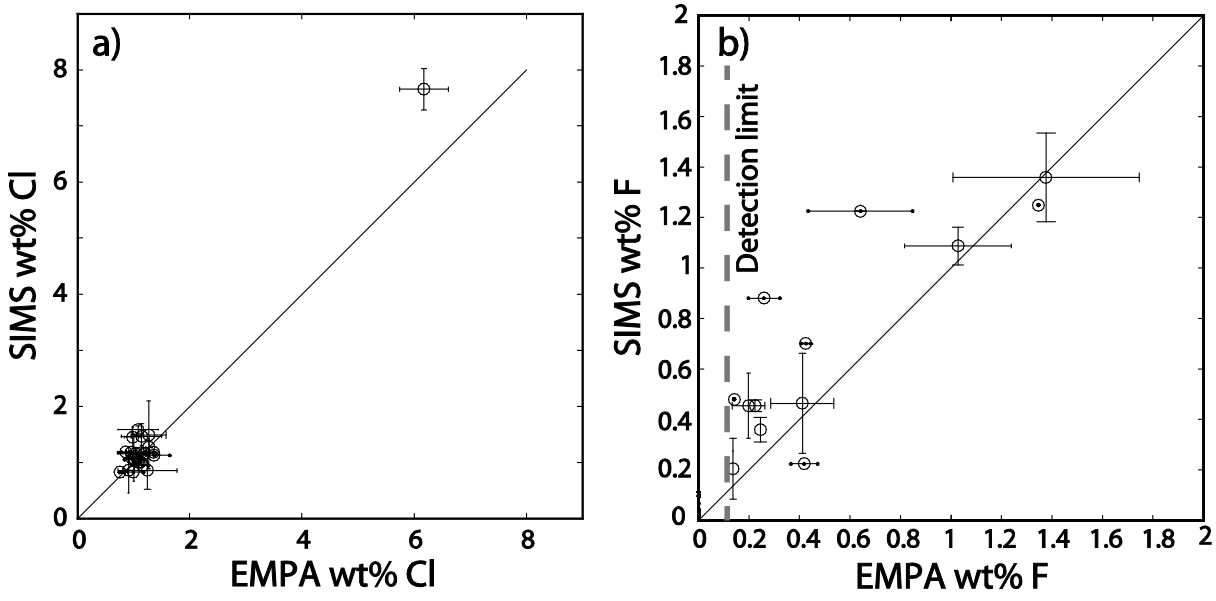


893

894 Fig. 5

895

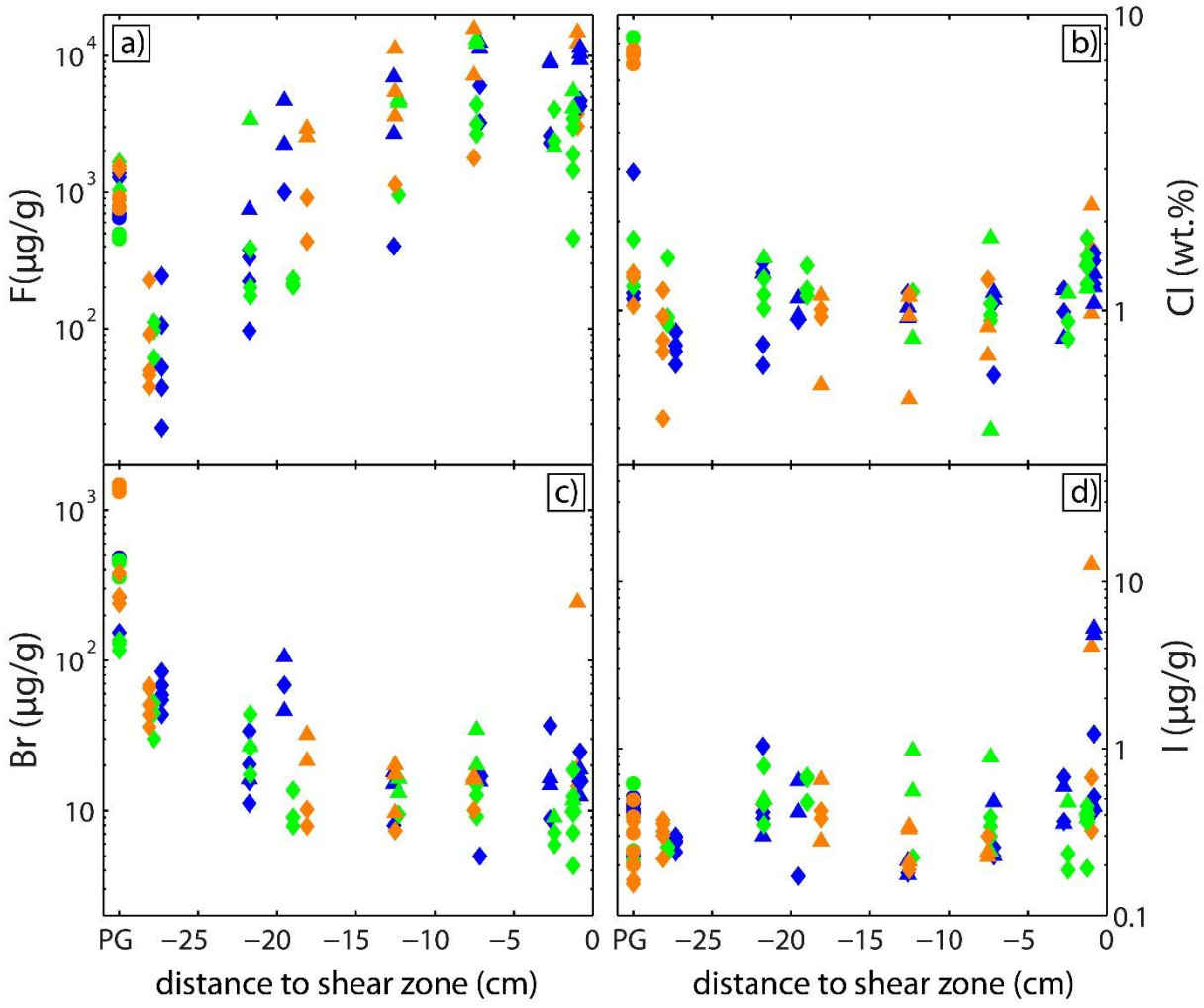
a)
b)
c)
d)
F(µg/g)
Cl (wt.%)
Br (µg/g)
I (µg/g)
PG
−25
−20
−15
−10
−5
0
distance to shear zone (cm)

Fig. 6

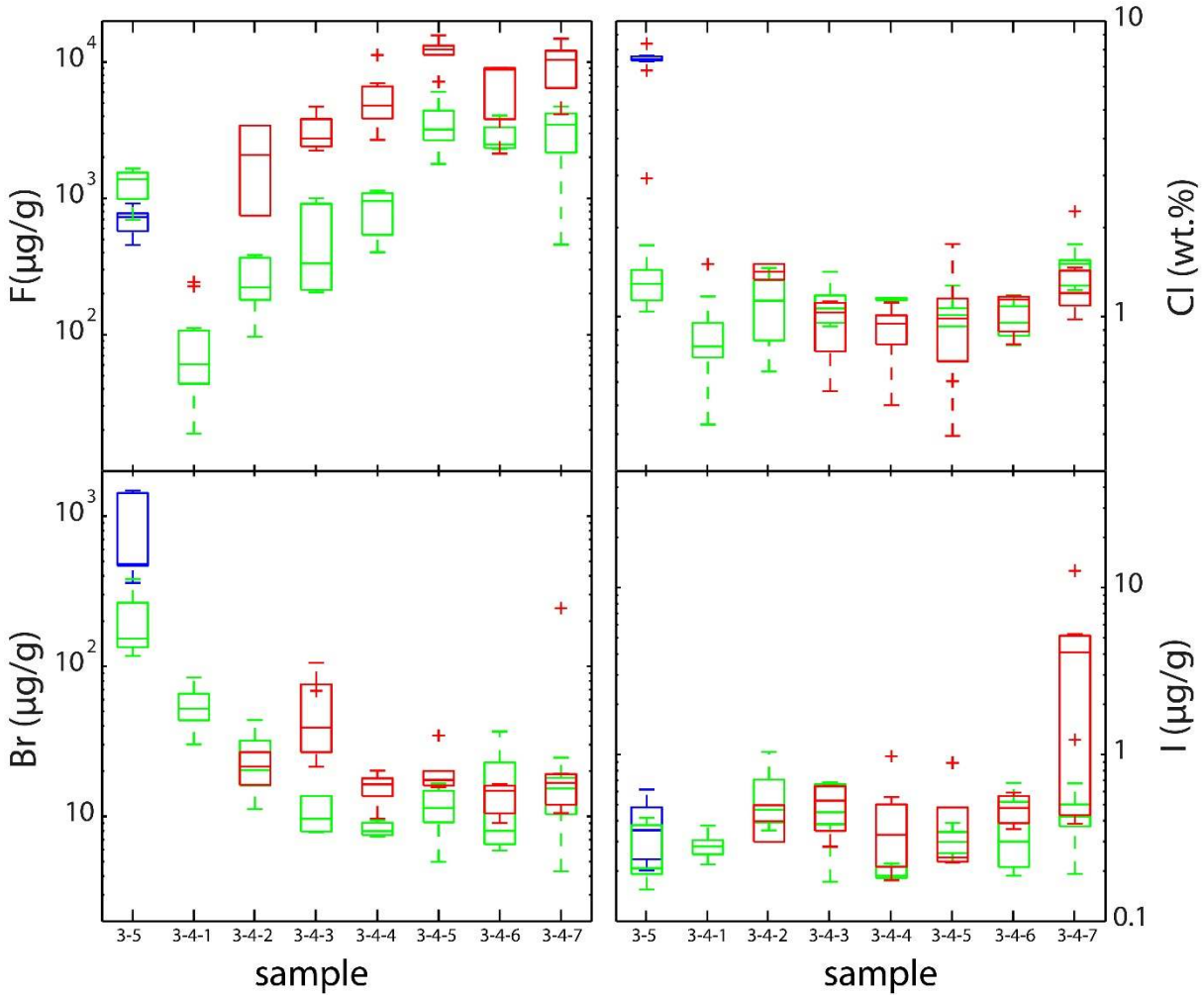


Fig. 7

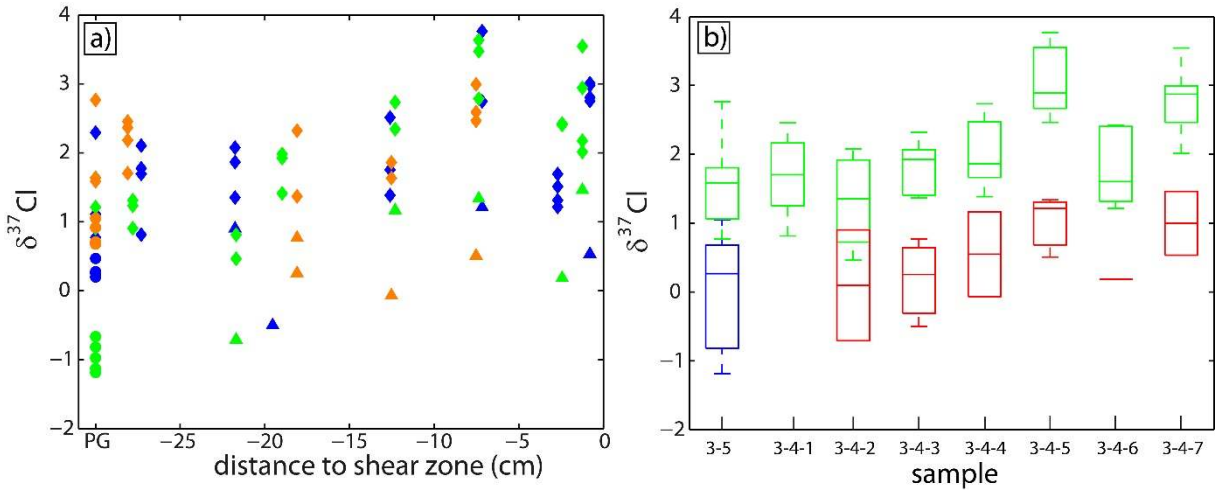


Fig. 8

Table 1: SIMS measurements of halogen concentrations and Cl stable isotopes

| Locality | sample | distance cm | Apatite | F (µg/g) | Cl (µg/g) | Br (µg/g) | I (µg/g) | Apatite | $\delta^{37}Cl$ ‰ | error |
|---|---|---|---|---|---|---|---|---|---|---|
| Bamble | BAM3-5_ap12_hal@1 | -30 | Cl-ap | 652 | 76380 | 482.7 | 0.23 | Cl-ap | 0.5 | 0.14 |
| Bamble | BAM3-5_ap12_hal@2 | -30 | Cl-ap | 678 | 76039 | 478.9 | 0.43 | Cl-ap | 0.3 | 0.14 |
| Bamble | BAM3-5_ap12_hal@3 | -30 | Cl-ap | 701 | 75406 | 473.0 | 0.51 | Cl-ap | 0.3 | 0.14 |
| Bamble | BAM3-5_ap12_hal@4 | -30 | Cl-ap | 776 | 75239 | 478.1 | 0.47 | Cl-ap | 0.2 | 0.14 |
| Bamble | BAM3-5_ap12_hal@5 | -30 | OH-ap | 1380 | 11233 | 153.1 | 0.20 | OH-ap | 0.8 | 0.15 |
| Bamble | BAM3-5_ap12_hal@6 | -30 | OH-ap | 696 | 30063 | 264.6 | 0.41 | OH-ap | 2.3 | 0.16 |
| Bamble | BAM3-5_ap12_hal@7 | -30 | OH-ap | 1285 | 11738 | 136.0 | 0.42 | OH-ap | 1.1 | 0.16 |
| Bamble | BAM3-5_ap8_hal@1 | -30 | Cl-ap | 496 | 75573 | 359.5 | 0.20 | Cl-ap | -1.2 | 0.14 |
| Bamble | BAM3-5_ap8_hal@2 | -30 | Cl-ap | 465 | 78140 | 465.8 | 0.62 | Cl-ap | -1.1 | 0.14 |
| Bamble | BAM3-5_ap8_hal@3 | -30 | Cl-ap | 454 | 85867 | 447.2 | 0.24 | Cl-ap | -1.0 | 0.14 |
| Bamble | BAM3-5-ap8-iso-cl@4 | -30 | | | | | | Cl-ap | -0.8 | 0.14 |
| Bamble | BAM3-5_ap8_hal@4 | -30 | OH-ap | 1659 | 17833 | 117.0 | 0.22 | OH-ap | 1.6 | 0.16 |
| Bamble | BAM3-5_ap8_hal@5 | -30 | OH-ap | 1028 | 12371 | 135.7 | 0.20 | OH-ap | 1.2 | 0.16 |
| Bamble | BAM3-5_ap8_hal@6 | -30 | OH-ap | 876 | 13204 | 129.0 | 0.21 | Cl-ap | -0.7 | 0.15 |
| Bamble | BAM3-5-ap8-iso-oh@4 | -30 | | | | | | OH-ap | 0.9 | 0.15 |
| Bamble | BAM3-5_ap1_hal@1 | -30 | Cl-ap | 916 | 74698 | 1410.2 | 0.31 | Cl-ap | 0.7 | 0.14 |
| Bamble | BAM3-5_ap1_hal@2 | -30 | Cl-ap | 779 | 77594 | 1483.1 | 0.49 | Cl-ap | 0.7 | 0.14 |
| Bamble | BAM3-5_ap1_hal@3 | -30 | Cl-ap | 774 | 76098 | 1445.1 | 0.20 | Cl-ap | 0.7 | 0.14 |
| Bamble | BAM3-5_ap1_hal@4 | -30 | Cl-ap | 757 | 77806 | 1480.6 | 0.24 | Cl-ap | 1.1 | 0.14 |
| Bamble | BAM3-5_ap1_hal@5 | -30 | OH-ap | 1546 | 13351 | 239.7 | 0.37 | OH-ap | 2.8 | 0.15 |
| Bamble | BAM3-5_ap1_hal@6 | -30 | OH-ap | 1461 | 13696 | 380.2 | 0.15 | Cl-ap | 0.9 | 0.15 |
| Bamble | BAM3-5_ap1_hal@7 | -30 | Cl-ap | 783 | 69678 | 1327.4 | 0.39 | OH-ap | 1.6 | 0.15 |
| Bamble | BAM3-5_ap1_hal@8 | -30 | OH-ap | 1544 | 10645 | 266.3 | 0.16 | OH-ap | 1.6 | 0.15 |
| Bamble | BAM3-4-1_ap1_hal@1 | -27.3 | OH-ap | 19 | 7812 | 43.7 | 0.24 | OH-ap | 0.8 | 0.09 |
| Bamble | BAM3-4-1_ap1_hal@2 | -27.3 | OH-ap | 37 | 7809 | 84.1 | 0.28 | OH-ap | 1.7 | 0.09 |
| Bamble | BAM3-4-1_ap1_hal@3 | -27.3 | OH-ap | 106 | 7450 | 54.6 | 0.30 | OH-ap | 2.1 | 0.09 |
| Bamble | BAM3-4-1_ap1_hal@4 | -27.3 | OH-ap | 52 | 8668 | 59.1 | 0.29 | OH-ap | 1.8 | 0.09 |
| Bamble | BAM3-4-1_ap1_hal@5 | -27.3 | OH-ap | 243 | 6729 | 68.2 | 0.27 | | | |
| Bamble | BAM3-4-1_ap2_hal@1 | -27.8 | OH-ap | 97 | 9232 | 44.5 | 0.26 | OH-ap | 1.3 | 0.09 |
| Bamble | BAM3-4-1_ap2_hal@2 | -27.8 | OH-ap | 112 | 9721 | 52.1 | 0.26 | OH-ap | 0.9 | 0.09 |
| Bamble | BAM3-4-1_ap2_hal@3 | -27.8 | OH-ap | 61 | 15409 | 30.1 | 0.24 | OH-ap | 1.2 | 0.09 |
| Bamble | BAM3-4-1_ap6_hal@1 | -28.1 | OH-ap | 49 | 4416 | 50.5 | 0.37 | OH-ap | 1.7 | 0.09 |
| Bamble | BAM3-4-1_ap6_hal@2 | -28.1 | OH-ap | 37 | 7427 | 43.6 | 0.22 | OH-ap | 2.2 | 0.09 |
| Bamble | BAM3-4-1_ap6_hal@3 | -28.1 | OH-ap | 227 | 9784 | 64.7 | 0.30 | OH-ap | 2.4 | 0.09 |
| Bamble | BAM3-4-1_ap6_hal@4 | -28.1 | OH-ap | 46 | 11988 | 68.2 | 0.36 | OH-ap | 2.5 | 0.10 |
| Bamble | BAM3-4-1_ap6_hal@5 | -28.1 | OH-ap | 91 | 8110 | 36.1 | 0.32 | | | |
| Bamble | BAM3-4-2_ap2_hal@1 | -21.76 | OH-ap | 333 | 6673 | 33.8 | 0.47 | OH-ap | 2.1 | 0.20 |
| Bamble | BAM3-4-2_ap2_hal@2 | -21.76 | OH-ap | 96 | 14948 | 20.3 | 0.42 | OH-ap | 1.9 | 0.20 |
| Bamble | BAM3-4-2_ap2_hal@3 | -21.76 | OH-ap | 222 | 7858 | 11.2 | 0.38 | OH-ap | 1.4 | 0.20 |
| Bamble | BAM3-4-2_ap2_hal@4 | -21.76 | F-ap | 744 | 13645 | 16.2 | 0.30 | F-ap | 0.9 | 0.20 |
| Bamble | BAM3-4-2_ap2_hal@5 | -21.76 | OH-ap | 378 | 13727 | 15.6 | 1.04 | | | |
| Bamble | BAM3-4-2_ap1_hal@1 | -21.7 | OH-ap | 383 | 10407 | 43.7 | 0.79 | OH-ap | 0.5 | 0.20 |
| Bamble | BAM3-4-2_ap1_hal@2 | -21.7 | OH-ap | 174 | 11580 | 26.3 | 0.47 | F-ap | -0.7 | 0.20 |
| Bamble | BAM3-4-2_ap1_hal@3 | -21.7 | OH-ap | 200 | 13132 | 17.3 | 0.35 | OH-ap | 0.8 | 0.20 |
| Bamble | BAM3-4-2_ap1_hal@4 | -21.7 | F-ap | 3420 | 15421 | 26.8 | 0.50 | | | |
| Bamble | BAM3-4-3_ap1_hal@1 | -19.54 | OH-ap | 1001 | 9476 | 68.5 | 0.17 | | -3.1 | 0.19 |
| Bamble | BAM3-4-3_ap1_hal@2 | -19.54 | F-ap | 2244 | 11277 | 46.1 | 0.64 | F-ap | -0.5 | 0.20 |
| Bamble | BAM3-4-3_ap1_hal@3 | -19.54 | F-ap | 4696 | 9878 | 105.4 | 0.42 | | | |
| Bamble | BAM3-4-3_ap4_hal@1 | -18.98 | OH-ap | 205 | 11490 | 7.9 | 0.68 | OH-ap | 2.0 | 0.20 |
| Bamble | BAM3-4-3_ap4_hal@2 | -18.98 | OH-ap | 213 | 14509 | 13.6 | 0.66 | OH-ap | 1.4 | 0.20 |
| Bamble | BAM3-4-3_ap4_hal@3 | -18.98 | OH-ap | 232 | 12071 | 9.0 | 0.48 | OH-ap | 1.9 | 0.20 |

| Locality | sample | distance cm | Apatite | F (µg/g) | Cl (µg/g) | Br (µg/g) | I (µg/g) | Apatite | $\delta^{37}Cl$ ‰ | error |
|---|---|---|---|---|---|---|---|---|---|---|
| Bamble | BAM3-4-3_ap6_hal@1 | -18.1 | OH-ap | 912 | 9751 | 7.9 | 0.38 | OH-ap | 1.4 | 0.24 |
| Bamble | BAM3-4-3_ap6_hal@2 | -18.1 | F-ap | 2551 | 5726 | 32.1 | 0.28 | F-ap | 0.8 | 0.24 |
| Bamble | BAM3-4-3_ap6_hal@3 | -18.1 | F-ap | 2944 | 11500 | 21.4 | 0.65 | F-ap | 0.3 | 0.24 |
| Bamble | BAM3-4-3_ap6_hal@4 | -18.1 | OH-ap | 435 | 10324 | 10.2 | 0.42 | OH-ap | 2.3 | 0.24 |
| Bamble | BAM3-4-4_ap4_hal@1 | -12.6 | OH-ap | 401 | 11744 | 8.0 | 0.18 | OH-ap | 1.4 | 0.20 |
| Bamble | BAM3-4-4_ap4_hal@2 | -12.6 | F-ap | 7013 | 10516 | 18.1 | 0.21 | OH-ap | 1.8 | 0.20 |
| Bamble | BAM3-4-4_ap4_hal@3 | -12.6 | F-ap | 2685 | 9706 | 15.1 | 0.18 | OH-ap | 2.5 | 0.20 |
| Bamble | BAM3-4-4_ap6_hal@1 | -12.3 | F-ap | 4790 | 8248 | 16.4 | 0.98 | OH-ap | 2.7 | 0.20 |
| Bamble | BAM3-4-4_ap6_hal@2 | -12.3 | OH-ap | 954 | 11861 | 9.5 | 0.22 | OH-ap | 2.3 | 0.20 |
| Bamble | BAM3-4-4_ap6_hal@3 | -12.3 | F-ap | 4538 | 8251 | 13.2 | 0.55 | F-ap | 1.2 | 0.20 |
| Bamble | BAM3-4-4_ap5_hal@1 | -12.52 | OH-ap | 1133 | 11601 | 7.3 | 0.19 | OH-ap | 1.9 | 0.20 |
| Bamble | BAM3-4-4_ap5_hal@2 | -12.52 | F-ap | 3625 | 9812 | 9.7 | 0.21 | OH-ap | 1.6 | 0.20 |
| Bamble | BAM3-4-4_ap5_hal@3 | -12.52 | F-ap | 5458 | 11430 | 17.4 | 0.33 | F-ap | -0.1 | 0.20 |
| Bamble | BAM3-4-4_ap5_hal@4 | -12.52 | F-ap | 11237 | 5134 | 20.2 | 0.34 |  | 0.3 | 0.20 |
| Bamble | BAM3-4-5_ap6_hal@1 | -7.16 | OH-ap | 3233 | 10927 | 5.0 | 0.23 | OH-ap | 3.8 | 0.09 |
| Bamble | BAM3-4-5_ap6_hal@2 | -7.16 | OH-ap | 6035 | 6189 | 16.5 | 0.26 | F-ap | 1.2 | 0.09 |
| Bamble | BAM3-4-5_ap6_hal@3 | -7.16 | F-ap | 12492 | 11795 | 15.7 | 0.48 | OH-ap | 2.7 | 0.09 |
| Bamble | BAM3-4-5_ap6_hal@4 | -7.16 | F-ap | 11291 | 11173 | 18.1 | 0.23 |  |  |  |
| Bamble | BAM3-4-5_ap5_hal@1 | -7.36 | OH-ap | 4405 | 9905 | 9.1 | 0.30 | OH-ap | 3.5 | 0.09 |
| Bamble | BAM3-4-5_ap5_hal@2 | -7.36 | OH-ap | 3155 | 9481 | 12.7 | 0.39 | OH-ap | 3.6 | 0.09 |
| Bamble | BAM3-4-5_ap5_hal@3 | -7.36 | OH-ap | 2669 | 10809 | 14.8 | 0.34 | OH-ap | 2.8 | 0.09 |
| Bamble | BAM3-4-5_ap5_hal@4 | -7.36 | F-ap | 12247 | 18041 | 20.0 | 0.89 | F-ap | 1.3 | 0.11 |
| Bamble | BAM3-4-5_ap5_hal@5 | -7.36 | F-ap | 13204 | 4040 | 34.6 | 0.24 |  |  |  |
| Bamble | BAM3-4-5_ap4_hal@1 | -7.52 | OH-ap | 1783 | 13038 | 10.1 | 0.30 | OH-ap | 2.6 | 0.09 |
| Bamble | BAM3-4-5_ap4_hal@2 | -7.52 | F-ap | 7180 | 9023 | 16.0 | 0.24 | OH-ap | 3.0 | 0.09 |
| Bamble | BAM3-4-5_ap4_hal@3 | -7.52 | F-ap | 15728 | 7218 | 16.8 | 0.22 | F-ap | 0.5 | 0.11 |
| Bamble | BAM3-4-5_ap4_hal@4 | -7.52 |  |  |  |  |  | OH-ap | 2.5 | 0.09 |
| Bamble | BAM3-4-6_ap4_hal@1 | -2.7 | F-ap | 8805 | 8258 | 14.8 | 0.36 | OH-ap | 1.5 | 0.20 |
| Bamble | BAM3-4-6_ap4_hal@2 | -2.7 | OH-ap | 2298 | 10125 | 8.8 | 0.37 | OH-ap | 1.7 | 0.20 |
| Bamble | BAM3-4-6_ap4_hal@3 | -2.7 | OH-ap | 2601 | 12090 | 36.8 | 0.67 | OH-ap | 1.3 | 0.20 |
| Bamble | BAM3-4-6_ap4_hal@4 | -2.7 | F-ap | 9096 | 12039 | 16.4 | 0.59 | OH-ap | 1.2 | 0.20 |
| Bamble | BAM3-4-6_ap10_hal@1 | -2.44 | OH-ap | 2374 | 8207 | 5.9 | 0.19 | F-ap | 0.2 | 0.20 |
| Bamble | BAM3-4-6_ap10_hal@2 | -2.44 | OH-ap | 4050 | 9415 | 7.1 | 0.23 | OH-ap | 2.4 | 0.20 |
| Bamble | BAM3-4-6_ap10_hal@3 | -2.44 | F-ap | 2134 | 11695 | 9.0 | 0.48 | OH-ap | 2.4 | 0.20 |
| Bamble | BAM3-4-7_ap5_hal@1 | -0.96 | OH-ap | 3044 | 15458 | 14.5 | 0.32 |  |  |  |
| Bamble | BAM3-4-7_ap5_hal@2 | -0.96 | OH-ap | 3965 | 15531 | 18.3 | 0.67 |  |  |  |
| Bamble | BAM3-4-7_ap5_hal@3 | -0.96 | F-ap | 12347 | 10013 | 19.2 | 4.10 |  |  |  |
| Bamble | BAM3-4-7_ap5_hal@4 | -0.96 | F-ap | 14834 | 23251 | 244.0 | 12.62 |  |  |  |
| Bamble | BAM3-4-7_ap5_hal@5 | -0.96 | OH-ap | 3761 | 16598 | 17.3 | 0.46 |  |  |  |
| Bamble | BAM3-4-7_ap1_hal@1 | -0.8 | OH-ap | 4645 | 12569 | 15.3 | 1.22 | OH-ap | 2.8 | 0.16 |
| Bamble | BAM3-4-7_ap1_hal@2 | -0.8 | OH-ap | 4713 | 15063 | 16.2 | 0.51 | OH-ap | 3.0 | 0.16 |
| Bamble | BAM3-4-7_ap1_hal@3 | -0.8 | OH-ap | 4282 | 15986 | 24.6 | 0.43 | OH-ap | 3.0 | 0.16 |
| Bamble | BAM3-4-7_ap1_hal@4 | -0.8 | F-ap | 10340 | 10817 | 16.7 | 4.81 | F-ap | 0.5 | 0.16 |
| Bamble | BAM3-4-7_ap1_hal@5 | -0.8 | F-ap | 11401 | 12308 | 18.8 | 5.27 | OH-ap | 2.8 | 0.16 |
| Bamble | BAM3-4-7_ap1_hal@6 | -0.8 | F-ap | 9298 | 13663 | 12.5 | 0.45 |  |  |  |
| Bamble | BAM3-4-7_ap2_hal@1 | -1.24 | OH-ap | 459 | 14383 | 4.3 | 0.19 | OH-ap | 2.0 | 0.17 |
| Bamble | BAM3-4-7_ap2_hal@2 | -1.24 | OH-ap | 3463 | 17981 | 12.4 | 0.45 | OH-ap | 3.5 | 0.16 |
| Bamble | BAM3-4-7_ap2_hal@3 | -1.24 | OH-ap | 1894 | 12593 | 7.1 | 0.37 | OH-ap | 2.2 | 0.17 |
| Bamble | BAM3-4-7_ap2_hal@4 | -1.24 | OH-ap | 2970 | 15655 | 18.6 | 0.39 | OH-ap | 2.9 | 0.19 |
| Bamble | BAM3-4-7_ap2_hal@5 | -1.24 | F-ap | 4133 | 14985 | 11.7 | 0.38 | F-ap | 1.5 | 0.16 |

| | | | | | | | | | | |
|---|---|---|---|---|---|---|---|---|---|---|
| Bamble | BAM3-4-7_ap2_hal@6 | -1.24 | OH-ap | 1448 | 12576 | 9.6 | 0.39 | | | |
| Bamble | BAM3-4-7_ap2_hal@7 | -1.24 | F-ap | 5498 | 12206 | 10.5 | 0.43 | | | |
| Locality | sample | distance cm | Apatite | F (μg/g) | Cl (μg/g) | Br (μg/g) | I (μg/g) | Apatite | $\delta^{37}$Cl ‰ | error |
| OdegardensVerk | | | F-Cl-ap | 24524 | 20920 | 214.3 | 0.72 | F-Cl-ap | -0.4 | 0.28 |
| OdegardensVerk | 2 | | F-Cl-ap | 24578 | 18317 | 315.0 | 0.75 | F-Cl-ap | -0.5 | 0.28 |
| OdegardensVerk | 3 | | F-Cl-ap | 23705 | 22586 | 339.2 | 0.69 | F-Cl-ap | -0.7 | 0.28 |
| OdegardensVerk | | | | | | | | F-Cl-ap | -1.1 | 0.28 |
| OdegardensVerkGab | | | | | | | | F-Cl-ap | -0.7 | 0.28 |
| OdegardensVerkS1O42_ap_a@1 | | | | | | | | F-Cl-ap | -0.7 | 0.22 |
| OdegardensVerkS1O42_ap_a@2 | | | | | | | | F-Cl-ap | -0.4 | 0.22 |
| OdegardensVerkS1O42_ap_a@3 | | | | | | | | F-Cl-ap | -0.8 | 0.21 |
| OdegardensVerkS1O42_ap_a@4 | | | | | | | | F-Cl-ap | -0.8 | 0.22 |
| OdegardensVerkS1O42_ap_a@5 | | | | | | | | F-Cl-ap | -0.9 | 0.21 |
| OdegardensVerkS1O42_ap_a@6 | | | | | | | | F-Cl-ap | -0.7 | 0.21 |
| OdegardensVerkS1O42_ap_a@7 | | | | | | | | F-Cl-ap | -1.2 | 0.21 |
| OdegardensVerkS1O42_ap_a@8 | | | | | | | | F-Cl-ap | -0.9 | 0.21 |
| OdegardensVerkS1O42_ap_a@9 | | | | | | | | F-Cl-ap | -0.9 | 0.21 |
| OdegardensVerk | AE1 | | Cl-ap | 94 | 112406 | 23.8 | 0.25 | Cl-ap | 0.9 | 0.24 |
| OdegardensVerk | AE2 | | Cl-ap | 74 | 107357 | 23.5 | 0.22 | Cl-ap | 0.9 | 0.24 |
| OdegardensVerk | AE3 | | Cl-ap | 100 | 110363 | 23.4 | 0.22 | Cl-ap | 0.8 | 0.24 |
| OdegardensVerk | AE4 | | OH-ap | 6589 | 18640 | 20.0 | 0.34 | | | |
| OdegardensVerk | AE5 | | OH-ap | 10998 | 10238 | 27.8 | 0.39 | Cl-ap | 0.7 | 0.24 |
| OdegardensVerk | AE6 | | OH-ap | 2550 | 19107 | 22.8 | 0.25 | OH-ap | 1.1 | 0.24 |
| OdegardensVerk | AE7 | | Cl-ap | 83 | 104415 | 20.9 | 0.24 | OH-ap | 1.7 | 0.24 |
| OdegardensVerk | AE8 | | OH-ap | 2912 | 20579 | 28.5 | 0.48 | OH-ap | 1.5 | 0.24 |
| OdegardensVerkodegarden_iso | | | | | | | | OH-ap | 1.4 | 0.24 |
| OdegardensVerk 1059-45@1 | | | | | | | | Cl-ap | 0.9 | 0.21 |
| OdegardensVerk 1059-45@2 | | | | | | | | Cl-ap | 0.8 | 0.21 |
| OdegardensVerk 1059-45@3 | | | | | | | | OH-ap | 1.3 | 0.22 |
| OdegardensVerk 1059-45@4 | | | | | | | | OH-ap | 1.2 | 0.22 |
| OdegardensVerk 1059-45@5 | | | | | | | | Cl-ap | 0.7 | 0.21 |
| OdegardensVerk 1059-45@6 | | | | | | | | Cl-ap | 0.8 | 0.21 |
| OdegardensVerk 1059-45@7 | | | | | | | | OH-ap | 1.1 | 0.22 |
| OdegardensVerk 1059-45@8 | | | | | | | | OH-ap | 1.2 | 0.22 |
| OdegardensVerk 1059-45@9 | | | | | | | | OH-ap | 1.3 | 0.22 |
| OdegardensVerk1059-45@10 | | | | | | | | Cl-ap | 0.8 | 0.21 |
| OdegardensVerkS26_halogens_110114@1 | | | F-ap | 33481 | 7533 | 8.5 | 0.63 | | | |
| OdegardensVerkS26_halogens_110114@2 | | | F-ap | 29599 | 9346 | 48.3 | 0.44 | | | |
| OdegardensVerkS26_halogens_110114@3 | | | F-ap | 22848 | 9034 | 2.4 | 0.53 | | | |
| OdegardensVerkS26_halogens_110114@4 | | | F-ap | 19471 | 7030 | 1.9 | 0.30 | | | |
| OdegardensVerkS26_halogens_110114@5 | | | F-ap | 27561 | 10610 | 46.2 | 0.44 | | | |
| OdegardensVerkS26_halogens_110114@6 | | | F-ap | 29225 | 13674 | 11.6 | 0.46 | | | |